MINISTRY OF EDUCATION
FEDERAL UNIVERSITY OF RIO GRANDE DO SUL
GRADUATE PROGRAM IN MECHANICAL ENGINEERING

EVALUATION OF THE TOTAL ABSORPTIVITY OF NON-GRAY SURFACES SUBJECTED BY INCIDENT THERMAL RADIATION TRAVELLING THROUGH PARTICIPATING MEDIA

by

Cesar Augusto Basso

Dissertation for the degree of
Master in Engineering

Porto Alegre, March 2022

EVALUATION OF THE TOTAL ABSORPTIVITY OF NON-GRAY SURFACES SUBJECTED BY INCIDENT THERMAL RADIATION TRAVELLING THROUGH PARTICIPATING MEDIA

by

Cesar Augusto Basso
Bachelor in Mechanical Engineering

A Dissertation submitted to the committee of the Graduate Program in Mechanical Engineering (PROMEC), from the Engineering School of the Federal University of Rio Grande do Sul (UFRGS), as part of the necessary requirements to obtain the degree of

Master in Engineering

Field of Study: Energy

Advisor: Prof. Dr. Francis Henrique Ramos França

Evaluation Committee:

Prof. Dr. Andrés Armando Mendiburu Zevallos.....PROMEC / UFRGS

Prof. Dr. Felipe Roman Centeno .....PROMEC / UFRGS

Prof. Dr. Luís Mauro Moura .....PUC-PR

Prof. Dr. Fernando Marcelo Pereira
Coordinator of PROMEC

Porto Alegre, March 2022

AKNOWLEDGMENTS

I would like to thank my girlfriend, Jessie, for all of the support and assist during my master's.

I would also like to thank my family for everything they done to me and incentivizing me to follow my undergraduate and graduate program choices.

I also express my appreciation for my colleagues Guilherme and Roberta, which invested a lor of their time helping me develop the codes employed in this study and also reviewing my dissertation.

I'm also very thankful of my supervisor, Prof. Francis França, for all the guidance during this research and for the all of the great insights provided for the development of this study.

And finally I would like to thank all of the members of the evaluation committee, for all of the contributions to the final version of this work.

RESUMO

O fenômeno de transferência de calor por radiação é de suma importância para processos que envolvem elevadas temperaturas, como a combustão. Desta forma, para problemas usuais de engenharia, como o projeto de fornalhas e câmaras de combustão, é essencial levar em consideração os efeitos da radiação nas etapas iniciais do desenvolvimento. Entretanto, problemas envolvendo radiação térmica são complexos, ainda mais caso envolva meios participantes, como o dióxido de carbono e vapor de água, que são produtos da combustão. Para a solução deste tipo de problema, pode ser utilizado o método linha por linha (LBL), que é extremamente custoso computacionalmente devido ao elevado refinamento que exige na discretização espectral. Pode-se também empregar modelos globais para a solução, como é o caso da soma-ponderada-de-gases-cinza (WSGG). Este método possui uma acurácia com frequência muito boa para a representação de problemas envolvendo gases participantes e paredes negras. Entretanto, como no cálculo via WSGG não são conhecidas as propriedades espectrais dos gases participantes, para a representação de paredes não-cinza ocorrem divergências consideráveis contra o resultado exato, LBL. Para isso, metodologias começaram a ser desenvolvidas para contornar esta limitação. Uma delas é a adoção de uma temperatura de referência para a estimativa da absortividade da superfície não-cinza. Esta temperatura de referência foi arbitrada em estudos encontrados na literatura, trazendo bons resultados para problemas unidimensionais. A falta de um estudo aprofundado da influência das condições de contorno do problema motivou o presente estudo. Foram estudados três cenários distintos para os perfis de temperatura. A primeira com um perfil de temperatura simétrico, a segunda para perfis assimétricos, com temperatura máxima afastada da superfície não-cinza e a terceira com a temperatura máxima mais próxima da superfície. Foram avaliadas três diferentes propriedades da superfície e quatro diferentes misturas de gases participantes para cada cenário. Diferentes temperaturas de referência foram avaliadas para cada caso, com base nas temperaturas de cada perfil, buscando estimar com a maior acurácia os resultados da absortividade exata, calculada pelo método LBL. Os resultados se mostraram interessantes, visto que para todos os, foram encontradas temperaturas de referência que obtiveram divergências menores do que 10% ao resultado exato.

Palavras-chave: radiação; combustão; simulação, transferência de calor.

ABSTRACT

Heat transfer by radiation is of high importance for all processes that suffer the influence of high temperatures, such as combustion. Therefore, for usual engineering problems, such as the design of furnaces and combustion chambers, it is highly important to account for the thermal radiation effects at the initial stages of development. However, such problems are complex, and even more so if there is the presence of participating gases, such as carbon dioxide and water vapor, usual combustion products. For the solution of these problems, it can be employed the line-by-line (LBL) integration method, which is computationally expensive, due to its fine spectral discretization, but with it, provides results that are considered exact. Global models can also be employed for the solution of such problems, which is the case of the weighted-sum-of-gray-gases (WSGG) model. This solution method provides a good accuracy when compared to the benchmark solution when evaluating problems with participating media bound by black walls. However, due to the fact that when solving the WSGG model the spectral profile of the participating gases is not known, the representation of non-gray bounding walls is lackluster. To overcome this limitation, researchers started to develop methodologies that would allow the WSGG model to accurately represent non-gray walls. One of these methodologies is the adoption of a "reference temperature", for the estimation of the total absorptivity of the non-gray wall. In past studies, this reference temperature was arbitrated, providing good results for one-dimensional domains. The lack of studies evaluating in depth the influence of boundary conditions on these reference temperatures motivated this study. A total of three main scenarios were evaluated. The first with a non-uniform, symmetrical temperature profile, the second with asymmetrical temperature profiles, where the maximum temperature occurs away from the surface of interest, and the third, with the maximum temperature close to said surface. Three different spectral profiles were evaluated for the control surface, and also four different mixtures for the participating media. Different reference temperatures established from the temperature profiles, then these references were tested against the total absorptivity obtained by employing the LBL integration over the domain. The results proved to be interesting, where from the reference temperatures evaluated, it was found less than 10% of deviation to the exact solution.

Keywords: radiation; combustion; numerical simulation, heat transfer.

CONTENTS

LIST OF FIGURES

LIST OF TABLES

LIST OF ACRONYMS AND ABBREVIATIONS

CFD	Computational Fluid Dynamic
CW	Cumulative Wavenumber
DOM	Discrete Ordinates Method
FSCK	Full Spectrum Correlated *k*-distribution
FSK	Full Spectrum *k*-distribution
FVM	Finite Volume Method
GG	Gray Gas
HITEMP	High Temperature Molecular Spectroscopic Database
HITRAN	High-Resolution Transmission Molecular Absorption Database
LRT	Laboratório de Radiação Térmica
MSFSK	Multi Scale Full Spectrum *k*-distribution
MSMGFSK	Multi Scale Multi Group Full Spectrum *k*-distribution
RAM	Random Access Memory
RHS	Right Hand Side
RTE	Radiative Transfer Equation
SLW	Spectral Line Weighted-Sum-of-Gray-Gases
UFRGS	Federal University of Rio Grande do Sul
WSGG	Weighted-Sum-of-Gray-Gases

LIST OF SYMBOLS

Latin symbols

A	Area, m^2
B	Energy, W
C	Absorption cross section,
c	Speed of light in a vacuum, 2.998×10^8 m/s
C_1	First Planck constant, $0.59552137 \times 10^{-16}$ $W.m^2/sr$
C_2	Second Planck constant, 0.1437752 m.K
E	Emissive power, W/m^2
e	Energy level
F	Band emission factor
f	Weighing coefficient
h	Planck's Constant, 6.626×10^{-34} J.s
j	Emission coefficient
k	Thermal conductivity, W/m.K
m	Iteration number
M	Mass, kg
N_L	Loschmidt Number, $molecules/m^3$
P	Pressure, atm
Q	Total partition sum
r	Radial coordinate, m
R	Radius, m
S	Path length, m
s	Radiation path, m
v	Energy difference
V	Volume, m^3
x	Molar concentration, mol/m^3
Y	Molar fraction
I	Radiative intensity, $W/(m^2.sr)$
T	Temperature, K
n	Refractive index

Greek symbols

α	Absorptivity
γ	Absorption line half-width, m
Δ	Variation
ε	Emissivity
ζ	Non-dimension Planck constant
θ	Polar coordinate, control angle
κ	Absorption Coefficient, m^{-1}
λ	Wavelength, μm
σ	Stefan-Boltzmann constant, 5.670374419 $W/(m^2.K^4)$
φ	Azimuthal coordinate
η	Wavenumber, cm^{-1}
ν	Frequency, Hz

Subscripts

$(.)_{0\rightarrow\lambda T}$	Spectral range for the band emission factor
$(.)_{abs}$	Absorbed
$(.)_{avg}$	Average
$(.)_{b}$	Blackbody
$(.)_{c}$	Carbon Dioxide
$(.)_{c}$	Collision broadening
$(.)_{D}$	Doppler broadening
$(.)_{e}$	Emitted
$(.)_{em}$	Emission
$(.)_{i}$	Incident
$(.)_{i}$	Initial state
$(.)_{ij}$	State transition
$(.)_{j}$	Final State
$(.)_{k}$	Arbitrary spectral line
$(.)_{LBL}$	Line-by-line integration-based results
$(.)_{max}$	Maximum
$(.)_{n}$	Natural broadening
$(.)_{P}$	Photon
$(.)_{reb}$	Benchmark reference

$(.)_{ref}$ Reference

$(.)_{w}$ Water Vapor

$(.)_{w,avg}$ Arithmetic average between wall and gas properties

$(.)_{wall}$ Wall

$(.)_{\theta}$ Dependance on angle of incidence

$(.)_{\lambda}$ Spectral

Superscripts

$(.)^{e}$ East face

$(.)^{E}$ East point

$(.)^{P}$ Central point

$(.)^{w}$ West face

$(.)^{W}$ West point

$(.)^{ww}$ West of west face

1. INTRODUCTION

Over the years, the increase of computational power has been significant, making it possible the usage of numerical simulation in various steps of engineering design. However, even with these technological advancements, it is still very difficult to simulate the effects of thermal radiation in larger scales within participating media, without compromising the results. These applications match common engineering problems, such as the design of burners, ovens, furnaces and its flues. These devices operate at high temperatures and handle gases that are not transparent to radiation. Also, in recent years there has been great concern over energy production from nonrenewable sources, such as fossil fuels and its impact on the environment. Therefore, the proper design of these systems, aiming at higher degrees of efficiency is of high interest; numerical simulation of these processes can take part on this effort.

For the correct design of these devices, the thermal radiation must be correctly accounted for. However, due to the directional and spectral dependence of thermal radiation transfer, the solution of the radiative intensity field, if done by the line-by-line integration, is excessively time consuming. To obtain the most accurate result, hundreds of thousands of spectral lines must be evaluated, for every direction that the thermal radiation is transported. For larger three-dimensional models, the computational power required for the iterative development of some designs, can deem this approach non-feasible.

To overcome this, a number of models have been developed over the years, providing good accuracy at moderate computational times. The drawback of some of these models are their strict applicability, where not many can handle the behavior of participating media bound by non-gray walls, hampering the correct estimation of the intensity field and causing deviations from the exact solution.

In recent years, some models were developed aiming to improve the solution of the intensity field on domains bounded by non-gray walls, with greater accuracy and less computational resources. Some of the most notable studies are discussed in the next section.

1.1 LITERATURE REVIEW

Over the years different methods to evaluate the heat transfer in participating media have been developed. These models aim to provide accurate results for the behavior of the heat transfer but without the computational resources required to solve the radiative transfer equation

(RTE) over the entire spectrum. This procedure deems the calculation of heat transfer problems difficult, time consuming and sometimes not feasible for common engineering problems.

One of the simplest models for the evaluation of heat transfer on participating media is the gray-gas (GG) model. This model is based on the replacement of all of the spectral information of the media by a single gray gas, hence the name. This model greatly reduces the computing time of the RTE when compared to the exact solution, due to the fact that there is no need to integrate over the spectrum. This reduces the total number of calculations performed. As one could expect, with the simplicity of the model, considerable discrepancy is normally observed when compared to an exact solution. A good application for this model is when the problem involves the presence of particulates suspended on the media, such as soot. These particulates have a much simple dependence on the spectrum as compared to gases. Therefore with moderate to high concentration of particles, the model can represent the thermal radiation more accurately (Fraga *et al.*, 2019). Recent developments of this model can be found on the works of, Centeno *et al.*, 2015, where the GG model was used to obtain the solution of the RTE in a computational fluid dynamics (CFD) code of turbulent non-premixed methane-air flames, with satisfactory results. Also, Fraga *et al.*, 2019, focused on the coupling of different GG model formulations to the Fire Dynamics Simulator, the work of Fernandes *et al.*, 2020 also performed a similar evaluation. Both of these studies proved the GG model to cost effective, providing good results with a small increment in computational effort, under the limitation that the medium is composed of adequate concentration of particulates.

The weighted-sum-of-gray-gases model, WSGG, replaces the spectral dependence of the media by a set of gray gases plus a gas transparent to radiation, namely the transparent windows. This model was first introduced by Hottel and Sarofim in 1967 and was only applicable to certain conditions, such as uniform temperature and concentrations of a domain. Further developments of the model were carried out by Smith *et al.*, 1982, where the study of different absorption coefficient polynomials was able to represent accurately a wide range of temperatures and pressures, as well as a mixture of different species. This provided a robust model to represent usual combustion problems.

A common limitation between these global models is that when calculating the RTE, the information regarding the spectral properties of the media is lost when developing the coefficients to use on the model. This is not a problem for the evaluation of domains bound by black walls, which is what these methods were first developed for. However, to evaluate non-gray walls, the spectral dependence of the media is required for the correct evaluation of the

thermal radiation. Therefore, to solve problems involving walls with non-gray behavior, there is the need to use more complex and time-consuming methods.

To overcome this limitation, many researchers tackled this problem by modifying existing solution methodologies or developed different models to solve the problem of participating media bounded by non-gray walls. Denison and Webb (1994) proposed a combination of the WSGG and *k*-distribution models. This so called "hybrid-model" combined the strengths of the two models, fast processing times for the WSGG and the accommodation of the spectral dependence of the *k*-distribution solution. The researchers obtained good agreement of the results when compared to the benchmark solution, line-by-line (LBL) integration over the spectrum, with great reduction in computing time. However, this method still proved to be more computationally expensive than the regular WSGG model.

Modest and Riazzi (2005) experimented with the relaxation of the full-spectrum *k*-distribution (FSK) model in order for it to perform calculations of a participating media surrounded by non-gray-walls. The method was based on grouping the spectral regions with similar properties, then solving a set of FSK solutions for the number of groups generated. By doing so, the possibility of obtaining solution of problems involving non-gray walls or even particles was achieved, but at a cost. The main disadvantage of the method was the necessity of creating several FSK bands over the spectrum, which can be cumbersome. This method also suffers from the same effect as the previous work discussed, where with the increase of the number of bands evaluated, the number of times the RTE must be solved increases accordingly.

In the following years further developments of the FSK model were carried, such as the one by Wang and Modest (2007), with a multi scale FSK (MSFSK) model. The authors pursued the effective modelling of thermal radiation in problems involving wall emission and absorption. This methodology requires the grouping of the individual spectral lines into a finite set of scales, according to their temperature and concentration dependence. By doing so, the RTE must be solved by the total number of scales configures in the analysis. This method has the benefit of achieving also good agreement with the benchmark solution (LBL). However, due to the nature of the MSFSK, the addition of the emission of the walls the user must calculate the scale overlaps by other means, such as the correlated-*k* (FSCK) approach, in order to achieve the aforementioned agreement with the benchmark. This procedure can be time consuming and cumbersome, and still do not provide good results in problems with inhomogeneous temperature and concentration profiles. Zhou *et al.* (2018) explored even further this method, by developing a different approach on how the grouping strategy is handled by the method, named MSMGFSK model. The results showed an improvement in accuracy when dealing with

inhomogeneous media, at an increase of complexity. In order to achieve the level of accuracy presented in the papers, the user must perform different grouping strategies depending on the composition and thermodynamic state of the mixture.

Authors have also made modification to the cumulative wavenumber method (CW) for it to account the non-gray properties of walls. This model comprises in the creation of a linear absorption cross-section function, where its value is constant for regions in the spectrum where the absorption cross-section is below a certain value. Solovjov *et al.* (2013) modified the model by employing a similar approach to the spectral line WSGG (SLW), where part of the radiation is represented by a gray gas and another transparent one. The wall emissivity is possible to be implemented due to creation of different bands, where the radiation is evaluated. Despite the accuracy of this implementation, the mathematical model is quite computationally expensive.

From these studies, it is possible to observe that over the years, researches increased the level of complexity of the radiative heat transfer modelling to allow for accurate results on participating media bound by non-gray walls problems. Hence, with these higher degrees of complexity, comes higher pre-processing times of the spectral data, as well as higher computational time for the RTE. However, an investigation being carried out by the Thermal Radiation Laboratory (LRT) from the Federal University of Rio Grande do Sul (UFRGS) is proving a good correlation between modifications to WSGG and SLW methodologies with the LBL integration.

Da Fonseca *et al.* 2018 assessed the usage of the WSGG methodology for use on heat transfer over a participating media comprised of a mixture of CO_2 and H_2O bound by non-gray walls. The methodology consisted in the assumption that the absorption coefficient of the medium is be randomly spread over the entire spectrum, with an equal probability This provides a uniform energy being emitted by the gas over the spectral bands of the non-gray wall. Then the RTE is solved for each of the individual surface spectral emissivity bands, in order to account for the spectral bands of the bound walls. With this mathematical modelling, the researchers achieved a better agreement with the LBL solution, when compared to the same problem evaluated as bound by black and gray walls. The heat flux deviation from the LBL solution was reduced in one of the scenarios from 9% with the assumption of a gray wall, to 4.6% when the wall was assumed non gray. However, in another test case, there was a deviation increase with the methodology. The researchers noted that the estimation of the absorptivity equal to the emissivity at the wall temperature is not an adequate assumption for most scenarios, and that could provide larger deviations in some situations.

In 2019, Da Silva and colleagues implemented a modification to the SLW methodology, where it was assumed a reference state, for the computation of properties, such as the absorption cross section. This reference state is also used to compute the total hemispherical absorptivity, by the assumption of a diffuse surface. In this study, two reference temperatures were evaluated, the average temperature of the participating media, and the wall temperature. The group evaluated the heat flux and source terms over an unidimentional slab containing a mixture of CO_2 and H_2O, at 1 atm, subjected to non-uniform temperature distributions. From this methodology, and comparison to other studies, it was concluded that considering the reference state equal to the average temperature of the mixture provided better agreement with the LBL solution than when working with the wall temperature. The group found similar results that of Da Fonseca *et al.* 2018, where the methodology provided a better representation of the radiative transfer, when comparing to the black and gray wall handling.

Da Fonseca *et al.* in 2020 provided a deeper evaluation of the usage of reference temperatures for the estimation of the heat transfer over participating media, accounting for non-gray bounding walls. The main problem was solved assuming the reference temperature being a spatial average of the media temperature, following the work of Da Silva *et al.* 2019, for the calculation of the total hemispherical absorptivity. The method, called Grouping of Wall Bands (GWB), does not require the solution of the RTE for all of the spectral emissivity bands of the bounding surface, due to the calculation of the absorptivity, previously mentioned. The method provided good agreement with the LBL integration method, providing a reduction in computational time proportional to the number of the wall spectral bands, when compared to similar methods that evaluate the spectral bands separately. The group also evaluated the influence on the heat flux and source term deviations for a range of reference temperatures, which proved to impact greatly the final result, ranging from 2% deviation, up to 20%.

With the good accuracy of the results obtained in the aforementioned study and the relative efficiency in computational time, the present study proposes to evaluate the usage of the reference temperature, identifying possible methodologies for its calculation for different scenarios, comprising different temperature profiles, species concentrations and wall spectral properties.

1.2 OBJECTIVES

The main objective of this work is the evaluation of the reference temperature methodology for the prediction of the total absorptivity of a surface through the line-by-line integration method.

This study was motivated by the good agreement of the results proposed by Da Fonseca *et al.* in 2019 and 2020 and by Da Silva *et al.* in 2019. However, it is still necessary a better understanding of what is the most suitable reference temperature to be employed in different applications of heat transfer across participating media. The proposed scenario is a control surface enclosed by a black hemisphere, where this hemisphere is filled with a mixture of carbon dioxide and water vapor, which are opaque to thermal radiation. This study will evaluate different reference temperatures, calculate the total hemispherical absorptivity related to them and then compare these estimations to the exact absorptivity value provided by the LBL integration. The proposed scenarios evaluate three main temperature conditions. The first is when the temperature profile provides the highest temperature close to the surface of interest. The second is when the maximum temperature lies at the midpoint of the domain, with a symmetrical temperature distribution. The last one is when the temperature profile provided a maximum temperature closest to the black hemisphere. The error between the reference temperature methods will then be compared and a proposed usage for these reference values will be discussed.

This study aims to provide the required knowledge for the correct estimation of the reference temperature for the WSGG and SLW methodologies described in the last section. With the correct reference temperature estimation, it is possible to significantly reduce the deviation of the calculated total hemispherical absorptivity, and then achieving more accurate results for the radiative heat flux and source term, using the aforementioned methodologies.

1.3 OUTLINE OF THE WORK

This document is divided in five main chapters. The first one provides a review of the state of the art of radiation heat transfer in participating media bounded by non-gray walls.

The second chapter provides a technical review of the main aspects of heat transfer on participating media, and also a technical description and derivation of the methods employed to obtain the results presented in this study.

Chapter 3 details the methodology employed in the construction of this study. It details the studied domain, its characteristics, the proposed temperature distributions and also the boundary conditions of the problem.

The fourth chapter is dedicated to the presentation and explanations of the encountered results, determining the overall accuracy of the absorptivity predictions and their deviation from the exact solution (LBL). In this chapter it is also discussed the preferred temperatures based on the three main temperature scenarios investigated.

The fifth and final chapter provides the closing remarks from the study, compiling the main results and providing the final conclusions from this study. At the end of the document also the references used in this present work are also provided.

2. THERMAL RADIATION FUNDAMENTALS

2.1 BLACKBODY

The blackbody is an idealized definition of a body or surface, which serve as a baseline of comparison to define important properties of real surfaces. This idealization is based on three main assumptions. The first one is that the blackbody is a perfect absorber of thermal radiation, that is, independent of the temperature or the wavelength, all of the thermal radiation is absorbed by it, that is, the blackbody is *gray*. The second is that regardless of temperature or the wavelength at which is being evaluated, no other surface can emit more energy than the blackbody. And lastly, the blackbody is perfectly diffuse, which means that its emitted energy is directionally independent (Bergman; Lavine, 2017).

The spectral intensity of a blackbody, that is, the radiative energy emitted by the body at a given wavelength and solid angle, can be obtained by the Planck's Distribution. Therefore, for a given temperature T and wavelength λ, the blackbody spectral intensity can be obtained by (Howell; Mengüç; Siegel, 2012):

$$I_{\lambda,b}(\lambda,T)=\frac{E_{\lambda,b}(\lambda,T)}{\pi}=\frac{2C_1}{n^2\lambda^5\,[exp\left(\frac{C_2}{n\lambda T}\right)-1]} \tag{2.1}$$

where C_1 and C_2 are the first and second Planck constants, respectively and n is the refractive index of the medium. Equation 2.1 can also be manipulated and employed to be evaluated for wavenumbers, η and frequency, v. The spectral emissive power of a blackbody, E, is derived from the spectral intensity, where by dividing the intensity value by π, the radiation emitted by the blackbody over all directions is obtained.

Starting from Equation 2.1, one can integrate it over the entire spectrum in order to obtain the total emissive power from a blackbody. The Stefan-Boltzmann Law is then given by (Bergman; Lavine, 2017):

$$E_b(T)=\int_0^\infty E_{\lambda,b}\,d\lambda=\sigma T^4 \tag{2.2}$$

where σ is the Stefan-Boltzmann constant, equal to $5.670374419\text{x}10^{-8}$ W/m².K^4.

For the study presented in this work, the evaluated surfaces will be of the diffuse-gray type, that is, their properties are dependent of wavelength, but independent of direction.

2.1.1 Blackbody Radiation Within Spectral Bands

Besides calculating the total emissive power or at a specific wavelength of a blackbody, it is also important to determine the emissive power at a finite portion of the spectrum, or a band. This can be performed by the calculation of the emissive power fraction, F, which in summary is the integration of $E_{\lambda,b}$ between the desired spectral band over E_b (Howell; Mengüç; Siegel, 2012). A visual representation of this quantity is shown in Figure 2.1.

The calculation of F can be performed without dealing with the integration over the spectrum. By manipulating the Stefan-Boltzmann law, Equation 2.2, Chang and Rhee, 1984, developed the following infinite sum relation:

$$F_{0\rightarrow\lambda T}=\frac{15}{\pi^4}\sum_{m=1}^{\infty}\left[\frac{exp\,-m\zeta}{m}\left(\zeta^3+\frac{3\zeta^2}{m}+\frac{6\zeta}{m^2}+\frac{6}{m^3}\right)\right] \tag{2.3}$$

where m is the iteration number, and ζ is given by:

$$\zeta=\frac{C_2}{\lambda T} \tag{2.4}$$

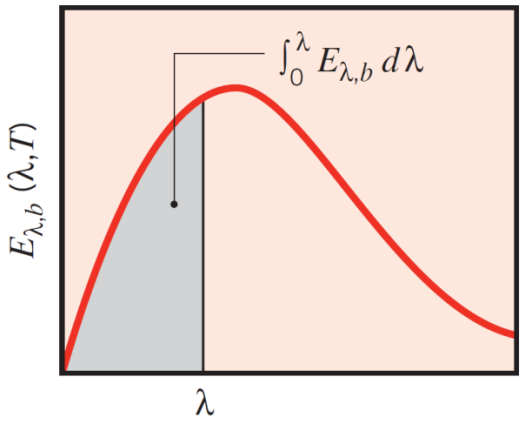

Figure 2.1 – Visual representation of the integration of the blackbody emissive power over a spectral band [Bergman et al. 2017].

2.2 SPECTRAL PROPERTIES OF REAL SURFACES

As mentioned in the previous subsection, the blackbody is a concept of an ideal emitter of radiative energy. The blackbody then, is used as a baseline of comparison between real world surfaces, since these surfaces differ from Planck's distribution, as observed in Figure 2.2(a). By this comparison, a number of definitions were developed in order to quantify the radiative properties of opaque surfaces, which will be described in the following sections.

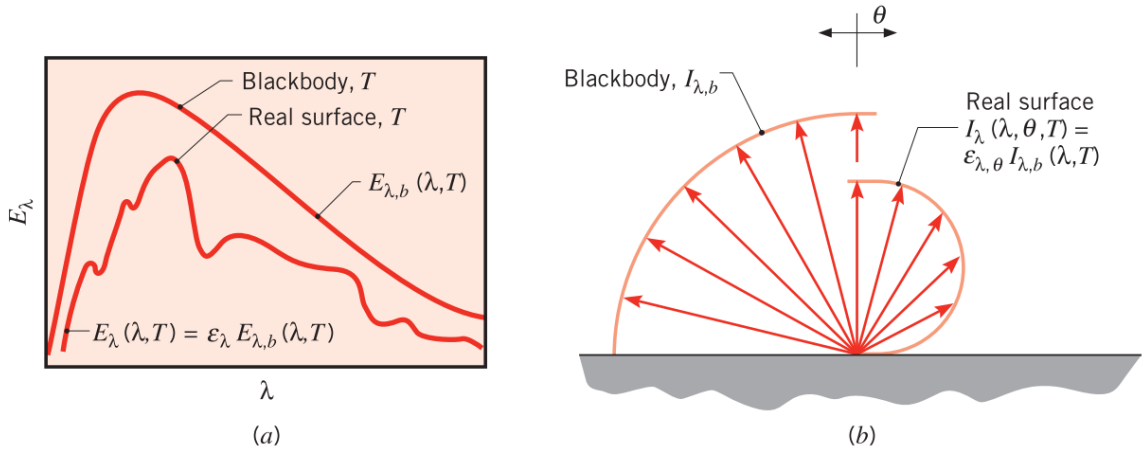

Figure 2.2 – (a) Comparison between the emitted radiative energy from a blackbody (Planck's distribution) and an arbitrary real surface. (b) Comparison between the blackbody diffuse nature and a non-diffuse real surface [Bergman et al. 2017].

Throughout this work, the standard nomenclature employed to the radiation properties are the following: directional spectral is a property function of the angle of incidence θ and the wavenumber η. Directional total is the integration of the property over the entire spectrum, still with dependence of the angle θ. Hemispherical total is the integration of the aforementioned property definition over all directions.

2.2.1 Emissivity

Emissivity, ε, is a property of real surfaces that specifies the amount of radiation intensity emitted by the surface, when compared to a blackbody at the same temperature (Howell; Mengüç; Siegel, 2012). The directional spectral emissivity can be found by employing: (Bergman; Lavine, 2017).

$$\varepsilon_{\lambda,\theta}(\lambda,\theta,\phi,T)=\frac{I_{\lambda,e}(\lambda,\theta,\phi,T)}{I_{\lambda,b}(\lambda,T)} \tag{2.5}$$

where θ is the polar angle, φ is the azimuthal angle, and the subscript e denotes the emitting real surface. From this definition, and also the definitions of the blackbody, one can observe that the emissivity can only vary between 0 and 1, where 0 would be a surface that provides zero emission of radiation energy, and 1 is a surface with blackbody characteristics.

By integrating Equation 2.5 over the spectrum, it is obtained the directional total emissivity:

$$\varepsilon_{\theta}(\theta,\phi,T)=\int_0^{\infty}\frac{I_{\lambda,e}(\lambda,\theta,\phi,T)}{I_{\lambda,b}(\lambda,T)}d\lambda=\frac{I_e(\theta,\phi,T)}{I_b(T)} \tag{2.6}$$

Finally, the hemispherical total emissivity is obtained by integrating Equation 2.6 over all directions, as following:

$$\varepsilon(T)=\int_0^{2\pi}\int_0^{\frac{\pi}{2}}\frac{I_e(\theta,\phi,T)\ cos\theta\ sin\theta\ d\theta\ d\phi}{I_b(T)\ \ cos\theta\ sin\theta\ d\theta\ d\phi} \tag{2.7}$$

$$E(T)=\varepsilon(T)E_b(T) \tag{2.8}$$

Equation 2.8 represents the derivation of the total emissive power of a surface at any given temperature.

2.2.2 Absorptivity

Absorptivity, unlike emissivity, is not technically a surface property, as it is dependent of the incident radiative intensity of the surface of interest. (Modest, M. F., 2013). The definition of the absorptivity is the fraction of the incident radiative energy that is absorbed by a body, and is independent of the surface temperature of said body (Howell; Mengüç; Siegel, 2012). The directional spectral absorptivity can then be obtained by:

$$\alpha_{\lambda,\theta}(\lambda,\theta,\ \phi)=\frac{I_{\lambda,i,abs}(\lambda,\theta,\phi)}{I_{\lambda,i}(\lambda,\theta,\ \phi)} \tag{2.9}$$

where α is the absorptivity, the subscripts *i* and *abs* denotes the incident radiation and the absorbed portion of this quantity, respectively. By the same procedure shown for the emissivity, one can integrate the directional spectral absorptivity over the entire spectrum in order to obtain the directional total absorptivity, described as:

$$\alpha_\theta(\theta,\ \phi)=\int_0^\infty \frac{I_{\lambda,i,abs}(\lambda,\theta,\phi)}{I_{\lambda,i}(\lambda,\theta,\ \phi)}d\lambda=\frac{\int_0^\infty \alpha_{\lambda,\theta}(\lambda,\theta,\ \phi)\,I_{\lambda,i}(\lambda,\theta,\ \phi)d\lambda}{\int_0^\infty I_{\lambda,i}(\lambda,\theta,\ \phi)\ d\lambda} \tag{2.10}$$

And for the evaluation of the total hemispherical absorptivity, that is, the absorptivity averaged over the entire spectrum and directions, the integration over all solid angles is performed on Equation 2.10, resulting in the following:

$$\alpha=\frac{\int_0^{2\pi}\int_0^{\frac{\pi}{2}} \alpha_\theta(\theta,\phi)\,I_i(\theta,\phi)\,cos\theta\,sin\theta\,d\theta\,d\phi}{\int_0^{2\pi}\int_0^{\frac{\pi}{2}} I_i(\theta,\ \phi)\ \ cos\theta\,sin\theta\,d\theta\,d\phi} \tag{2.11}$$

An important aspect in the evaluation of the absorptivity is its relation to the emissivity, specified by the Kirchhoff's Law. The most important one is that at the directional and spectral level, the absorptivity, $\alpha_{\lambda,\theta}$, is equal to the emissivity, $\varepsilon_{\lambda,\theta}$, at any thermodynamic condition. At the total directional level, the absorptivity α_θ, is only equal to the emissivity, ε_θ, for directional gray surfaces (Howell; Mengüç; Siegel, 2012).

2.3 THERMAL RADIATION IN PARTICIPATING MEDIA

A thermal radiation problem across a participating medium cannot be treated in the same manner as if the same problem was evaluated in a vacuum. The participating media, as the name implies, have direct influence of the radiation intensity incident to a body or a surface. This is common for engineering problems, such as combustion chambers, or any process that involves the consumption of fuels, where the combustions products can behave as a participating media (Modest, M. F., 2013). The molecules of the participating media, being gases or particles, may emit, absorb or scatter incident radiation. These phenomena will be detailed in the following sections, with the exception of scattering, which is outside the scope of this work.

2.3.1 Thermal radiation intensity

The spectral thermal radiation intensity, as briefly cited in the previous sections, is the spectral thermal radiation energy per unit projected area, per unit wavelength, per unit solid angle. The conventional units of this quantity is W/(m².µm.sr) (Howell; Mengüç; Siegel, 2012). The thermal radiation incident to a molecule or particle of the media can alter the amount of radiation of the particular path the rays were travelling along. This is caused by the distinct energy levels of the atoms in the molecules, where at specific levels, the atom can receive the impact of a incident photon and absorb its energy, therefore attenuating the intensity along the radiation path. Or, at a specific level, release a photon, which would consist in the augmentation of the incident ray (Modest, M. F., 2013).

2.3.2 Thermal radiation intensity attenuation – absorption

The total amount of radiation absorbed through the medium at a specific optical path is proportional to the magnitude of the energy and the length travelled by the radiation beam (Modest, M. F., 2013). By this definition, it is possible to describe the variation of intensity due to absorption as:

$$dI_{\eta,abs} = -\kappa_\eta I_\eta ds \tag{2.12}$$

where κ is the linear absorption coefficient and s is the radiation path. It is important to note that, since the radiation is being absorbed, i.e., attenuated, the negative sign on the right-hand-side of Equation 2.12 is present.

From the absorption coefficient, alongside the radiation intensity of the beam. One could be interested in the amount of radiation that is allowed across the participating media, based on the total amount of radiation that has been emitted. This relation is called transmissivity, and can be obtained by the following:

$$\tau_{0\rightarrow s} = \frac{\int_0^\infty I_{\eta,0}\ exp(-\bar{\kappa}_\eta S) d\eta}{I_0} \tag{2.13}$$

where, $\bar{\kappa}_\eta$ correspond to the average absorption coefficient along the path, *S* is the path length and the subscripts $0 \rightarrow s$ and *0* correspond to path from the emitting surface and the incident surface, respectively.

2.3.3 Thermal radiation intensity augmentation – emission

The radiation path that crosses a volume element, *dV*, of participating media, will gain energy by the form of emission, and this gain will be proportional by the size of said volume and also the length of the path. Under a local thermodynamic equilibrium (LTE), the intensity at any point in space must be equal to the blackbody intensity. Therefore we can specify the emission coefficient *j* (Howell; Mengüç; Siegel, 2012).

$$j_\eta(S,\theta,\phi)=\kappa_\eta I_{b\eta}(S) \tag{2.14}$$

Given this definition, it is possible to obtain the variation of intensity caused by emission along a small portion of the path, *ds.*

$$dI_{\eta,em}=\kappa_\eta I_{b\eta} ds \tag{2.15}$$

where the subscript *η,em* corresponds to the spectral emission term.

With the defined concepts of emission and absorption along a path, one can combine Equations 2.12 and 2.15 to form the radiative transfer equation (RTE) for an absorbing-emitting media, shown in Equation 2.16

$$\frac{dI_\eta}{ds}=\kappa_\eta(I_{b\eta}-I_\eta) \tag{2.16}$$

. The first term of the RHS of the equation corresponds to the augmentation due to emission and the second one to the attenuation due to absorption.

2.4 SPECTRAL LINE BROADENING

When studying the thermal radiation of participating media on common engineering problems, where the gases are not dissociated or ionized, the internal energy of the molecules have discrete states, being vibrational, rotational and electronic. If these molecules suffer the

impact of a photon, it is possible to occur an energy state transition. These transitions result in the absorption of said photons, which in turn appear as the lines of the transmission spectrum. The photon energy can be defined as:

$$e_P = e_j - e_i = hc\eta_{ij} \tag{2.17}$$

where e corresponds to the energy level, h is the Planck's constant, c is the speed of light in a vacuum and the subscripts P, j, i and ij correspond to the photon, arbitrary state j, arbitrary state i and the transition between states i and j, respectively (Howell; Mengüç; Siegel, 2012).

From Equation 2.17, one could conclude that the energy transition occurs at discrete wave numbers. However, due to the effect of some mechanisms, the influence of these "absorption lines", as they are called, do not limit at the discrete location on the spectrum. As will be discussed on the following subsections, these lines have the tendency to be "broadened", having a finite wave number span around the transition wave number η_{ij}. This broadened profile is shown in Figure 2.3.

The broadened profile shape is directly dependent on gas temperature, pressure and the length of the radiation path across this gas. In order to obtain the line intensity S_{ij} one could perform the integration of the absorption coefficient at the transition wave number, $\kappa_{\eta,ij}$ over the entire spectrum.

$$S_{ij} = \int_0^\infty \kappa_{\eta,ij} d\eta = \int_0^\infty \kappa_{\eta,ij} d(\eta - \eta_{ij}) \tag{2.18}$$

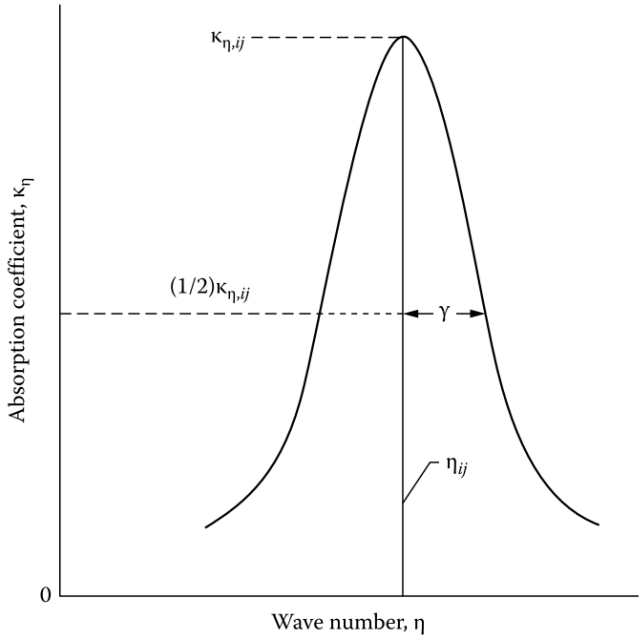

Figure 2.3 – Representation of the absorption line and the bell-shaped broadened profile. [Howell *et. al* 2013]

2.4.1 Natural broadening

The natural line broadening occurs at any stationary molecule, and it is caused by the uncertainty of the discrete energy levels of the molecules (Howell; Mengüç; Siegel, 2012). This is corroborated by the Heisenberg's uncertainty principle, where the energy transitions cannot occur with the same amount of energy every single time. Therefore the emission of energy varies slightly, causing the broadening (Modest, M. F., 2013). The natural line broadening shape can be obtained from:

$$\frac{\kappa_{\eta,ij}}{S_{ij}} = \frac{\frac{\gamma_n}{\pi}}{\gamma_n^2 + \left(\eta - \eta_{ij}\right)^2} \tag{2.19}$$

where γ_n is the line half-width at half-maximum of the natural broadening. The representation of γ_n can be seen on Figure 2.3. The shape of this broadening mechanism is the Lorentz profile.

For engineering applications, the natural broadening is usually neglected due to its small influence on the overall line broadening, when compared to the other mechanisms, that will be discussed shortly (Modest, M. F., 2013).

2.4.2 Doppler broadening

The Doppler effect, where waves can appear compressed to an observer if their emitter is moving towards the observer. And appear expanded if the emitter is moving away from the observer, can affect the absorption line shapes due to the inherent velocities of the molecules, called Maxwell-Boltzmann distribution velocities (Modest, M. F., 2013). The shape of this type of broadening can be described by:

$$\frac{\kappa_{\eta,ij}}{S_{ij}} = \frac{1}{\gamma_D}\sqrt{\frac{ln(2)}{\pi}}\,exp\left[-\left(\eta-\eta_{ij}\right)^2\frac{ln(2)}{\gamma_D^2}\right] \tag{2.20}$$

where γ_D is the line half-width of the Doppler broadening:

$$\gamma_D = \frac{\eta_{ij}}{c}\left(\frac{2kT}{M}ln(2)\right)^{\frac{1}{2}} \tag{2.21}$$

where k is the thermal conductivity of the molecule, T is the local temperature and M is the mass of the radiating molecule. The Doppler broadening is much more prominent at higher temperatures, as seen the term $T^{1/2}$ in Equation 2.21.

2.4.3 Collision broadening

The molecules of a gas are in constant collision between themselves and other molecules or particles present in the media. With the increase of pressure, the probability of these collisions is increased. The broadening of the spectral lines occurs due to the disturbance of the molecules energy levels caused by the collisions between molecules and this broadened profile can be obtained from a Lorentz profile (Howell; Mengüç; Siegel, 2012).

$$\frac{\kappa_{\eta,ij}}{S_{ij}} = \frac{\frac{\gamma_c}{\pi}}{\gamma_c^2+\left(\eta-\eta_{ij}\right)^2} \tag{2.22}$$

where the collision line half-width, γ_c is based on the molecule collision rate. Kinetic theory is employed to approximate the γ_c value:

$$\gamma_c = \frac{1}{2c} \frac{4D^2 P}{(\pi M k T)^{\frac{1}{2}}} \tag{2.23}$$

where D is the diameter of the molecules, P is the pressure of the gas and M is the mass of the individual molecule. From Equation 2.23, one can determine that at higher pressures and also lower temperatures, this broadening mechanism is of great importance. Also, for common engineering problems, such as combustion chambers, this mechanism is of such importance, that the others could be neglected in these analyses (Howell; Mengüç; Siegel, 2012).

2.4.4 Stark broadening

For situations where string electric fields are present, the energy levels of the surrounding molecules can be disturbed, causing large broadening of the spectral lines. In order to calculate the broadening caused by this mechanism, quantum mechanics shall be employed, with the results of highly asymmetrical profiles (Howell; Mengüç; Siegel, 2012).

2.5 SPECTRAL DATABASES

Over the years, databases containing the spectral data of a variety of molecular gases have been created, in order to provide a benchmark for engineering models when solving the radiative transfer equation. Despite the advancements in computing power, the high resolution of these databases makes them impractical to be used in common engineering applications (Howell; Mengüç; Siegel, 2012).

One of the pioneering compilations of spectral data was the one developed by the Cambridge's Air Force research laboratories in 1973 (Mcclatchey *et al.*, 1973). Where low temperature data for the constituents of significance of the earth's atmosphere was compiled, such as water vapor, carbon monoxide and dioxide, oxygen, ozone, methane and nitrous oxide.

This compilation was the basis for the current HITRAN database (Modest, M. F., 2013), which is currently in its 2020 version (Gordon *et al.*, 2021).

The High Resolution Transmission Molecular Absorption Database, HITRAN, is based on atmospheric data, and all the properties are referenced to the standard ambient temperature, 297K. Therefore, this database is not suitable for combustion problems, where the temperature of interest is much higher. Due to this limitations and the need for spectral data at higher temperatures from different research and industry sectors, the High Temperature Molecular Spectroscopic Database, HITEMP, database was created, analogous to HITRAN (Rothman *et al.*, 2010), being first released in 1995. Currently, the latest release of HITEMP is its 2010 version.

The HITEMP2010 database provide the line intensity of the molecular gases at different wavenumbers at the same reference temperature as HITRAN to maintain compatibility. Therefore this parameter must be adjusted to the temperature of interest (Rothman *et al.*, 2010). This can be done by solving the following:

$$S_k(T)=S_k(T_{ref})\frac{Q(T_{ref})}{Q(T)}\frac{exp\left(-\frac{C_2B_k}{T}\right)}{exp\left(-\frac{C_2B_k}{T_{ref}}\right)}\frac{\left[1-exp\left(-\frac{C_2\nu_k}{T}\right)\right]}{\left[1-exp\left(-\frac{C_2\nu_k}{T_{ref}}\right)\right]} \tag{2.24}$$

where Q is the total partition sums, T_{ref} is the reference temperature for the calculation, ν_k is the energy difference between the initial and final state and B_k is the energy of the lower state. The subscript k indicates the number of a given the spectral line

$$C_\eta(\eta)=\sum_{k=1}^{K}\frac{S_k(T)}{\pi}\frac{\gamma_k}{\gamma_k^2+(\eta-\eta_k)^2} \tag{2.25}$$

With the information of the line intensity at the corrected temperature, one can proceed to calculate the absorption cross section, C_η, given by the Lorentz profile, in Equation 2.25. A resulting spectral profile for C_η can be observed on Figure 2.4.

Then the absorption coefficient, κ_η can then be obtained, multiplying C_η by the Loschmidt number, N_L and the molar fraction, Y, of the molecular gas being evaluated, by the following relation: (Dorigon *et al.*, 2013).

$$\kappa_\eta = N_L Y C_\eta \tag{2.26}$$

With the pressure absorption coefficient, given in units of m^{-1} or cm^{-1} one can perform the solution of the radiative transfer equation, RTE.

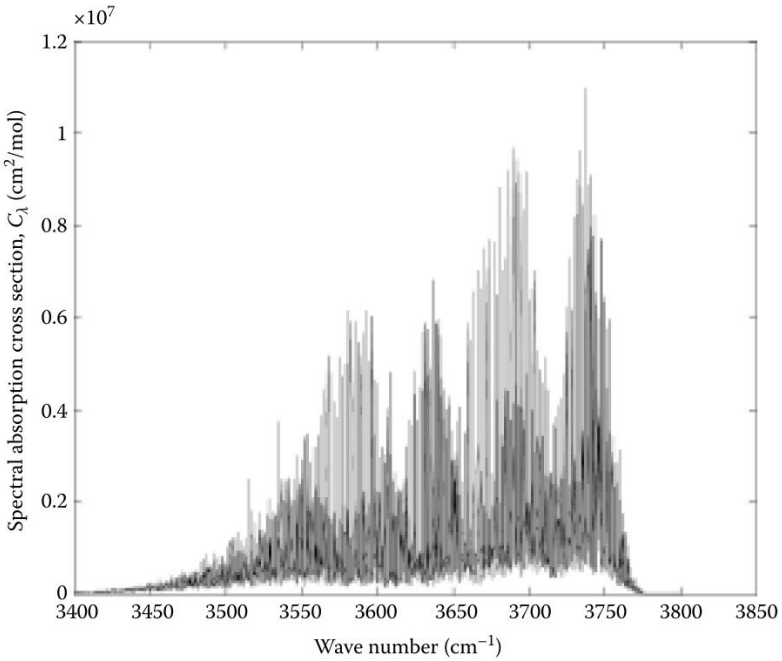

Figure 2.4 – Spectral absorption cross section for CO_2 at 1000K and 1atm for a portion of the spectrum [Howell *et al.* 2012]

2.6 THE RADIATIVE TRANSFER EQUATION

In order to determine the heat flux incident to a surface, or at any point of a opaque medium, the radiative intensity must be accounted for all directions and wavelengths (Modest, M. F., 2013). The intensity field is calculated by the means of the radiative transfer equation, or RTE. This equation correspond to the energy balance between the absorbing, emitting and scattering portions along a line of sight (Howell; Mengüç; Siegel, 2012).

The general configuration of the RTE, taking into account the absorbing, emitting and scattering terms is the following:

$$\frac{dI_\eta}{ds} = \kappa_\eta I_{b\eta} - \kappa_\eta I_\eta - \sigma_{s\eta} I_\eta + \frac{\sigma_{s\eta}}{4\pi} \int_0^{4\pi} I_\eta \Phi_\eta d\Omega_i \tag{2.27}$$

where, in the right-hand-side of the equation, the first term corresponds to the increase of energy by emission, the second the decrease by absorption, the third one is the energy lost by scattering and the last one the incident energy by scattering. By neglecting scattering, the equation reduces to the one already shown in Equation 2.16.

In order to obtain the radiative heat flux over a given surface, or any other point of the medium, there is the need to integrate Equation 2.27 or 2.16 over the entire spectrum and also over the radiation path. To perform such integration, boundary conditions must be specified, and for diffuse non-gray surfaces, are the following:

$$I_\eta(r=0)=\varepsilon_\eta I_{b,\eta}(r=0)+\frac{\alpha_\eta}{\pi}\int_0^{2\pi} I_\eta(r=0)cos\theta\ d\Omega_i \tag{2.28}$$

$$I_\eta(r=R)=\varepsilon_\eta I_{b,\eta}(r=R)+\frac{\alpha_\eta}{\pi}\int_0^{2\pi} I_\eta(r=R)cos\theta\ d\Omega_i \tag{2.29}$$

Equation 2.29, for the purposes of this work can be simplified for the condition of a black surface, with $\varepsilon_\eta = \varepsilon = 1$, becoming:

$$I_\eta(r=R)=\varepsilon_\eta I_{b,\eta}(r=R) \tag{2.30}$$

It is important to note that when observing the leftmost portion of the RHS of Equations 2.28 and 2.29, the incoming radiation must be known in order to solve the boundary condition equation. This imposes a challenge, where the intensity field on participating media is only known when the RTE is solved. Therefore, to solve problems involving participating media bound by non-gray walls, an iterative solution must be performed, increasing the computational cost of the solution.

2.7 SOLUTION METHODS OF THE RTE

Integration of the RTE over the spectrum is a challenging task, due to the close spacing between the spectral lines, which might have a considerable overlap istime consuming,due to the fact that, in order to represent the entire spectrum, hundreds of thousands of spectral lines are needed. There are different methods of spectrally integrate the RTE, such as narrow and wide band calculations and the employment of global models. However, the benchmark

solution, which gives the closest to the exact solution possible to date, remains the line-by-line integration. (Modest, M. F., 2013) This model is detailed in the following sub-section.

2.7.1 Line-by-line Integration

The line-by-line, LBL, integration of the spectral properties requires the use of the high-resolution spectral databases mentioned before, in Section 2.5. With these spectral databases in hand, one could develop a computational code in order to solve Equation 2.27 with great accuracy. However, with the highest degree of accuracy to date, comes a considerable computational cost of this method. In order to solve a problem by the LBL integration, every single spectral line must be evaluated for a given spectrum portion. This could translate do hundreds of thousands of times, that the RTE have to be solved in order to achieve the final solution (Modest, M. F., 2013).

Despite the computational costs of this method, it is constantly used as the benchmark solution to compare the accuracy of approximate spectral models. Examples of this are the evaluation of global models, in the works of Modest and Singh, 2005; Dorigon *et al.* 2013; Bordbar and Hyppänen, 2018; Centeno *et al.* 2018; Fonseca *et al.* 2020 and many others.

2.7.2 Spatial Integration of the RTE

From Equation 2.27, it is possible to observe the spatial dependence of the RTE. Therefore, in order to obtain the solution of radiation problems, there is the need to integrate the RTE over the spatial domain. Many methods were developed to obtain the spatial intensity fields, but the most prominent that are in use today are the discrete-ordinates-method (DOM) and the finite-volume-method (FVM). The advantage of these models is their robustness, providing accurate results for a wide range of problems, as well as the simplicity to implement them on CFD codes. (Coelho, 2014; Liu *et al.*, 2020).

The discretization of a participating media domain can be executed by different means, for either DOM or FVM methods. For an arbitrary hemispherical domain, one of the most simple and effective methods for the angular discretization by the FVM, which lies in the scope of this work, is by dividing the domain by a finite number of solid angles, or control angles (Coelho, 2014). This creates a set of non-overlapping “pencil” regions that represent the domain. Figure 2.5 presents a visual aid for the angular discretization of the FVM.

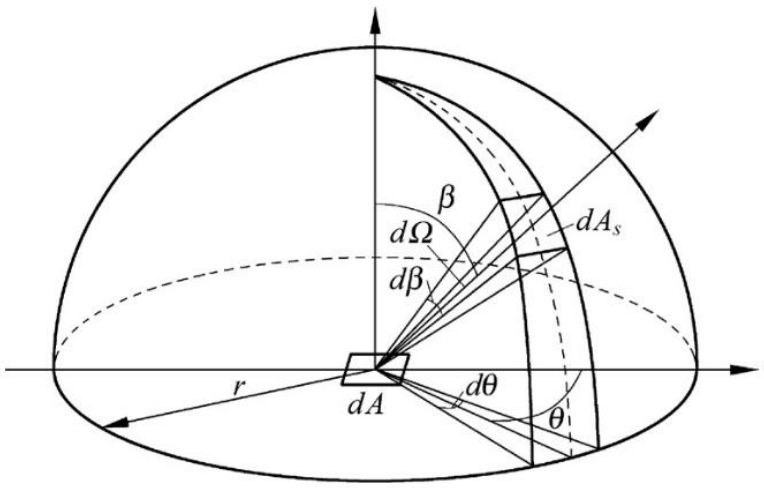

Figure 2.5 – Visual representation of the solid angle discretization for the FVM [Zhang *et al.* 2016].

One can see that for the half-hemisphere of radius *r*, presented on Figure 2.5, the discretized solid angle $d\Omega$ is composed of the polar segment $d\theta$ and the azimuthal segment $d\beta$. In a case of a hemisphere at a different thermodynamic state than the control surface *dA*, the finite area dA_s of the hemisphere will absorb or emit thermal radiation. The effective area of this surface is $r^2 cos\theta d\theta d\beta$.

2.8 THE FINITE VOLUME METHOD

The finite volume method, applied to thermal radiation uses the same principle as it is employed for diffusion and convection problems. This method performs the exact integration of the RTE over a line of sight and is fully conservative, therefore there are no loss in intensity or thermal energy (Modest, Michael F., 2013).

In order to perform this integration, first the line of sight of interest must be divided into segments of equal length. A general view of this division can be seen on Figure 2.6. Arbitrary names were given to the discretized nodal points of the domain in order to aid in the explanation. Let's say that a beam of thermal radiation is travelling from point A to point B in Figure 2.6. Then, the point named *P* is the current point where the RTE is being calculated, *W* is the point upstream from *P*, and *E* is the point downstream from it.

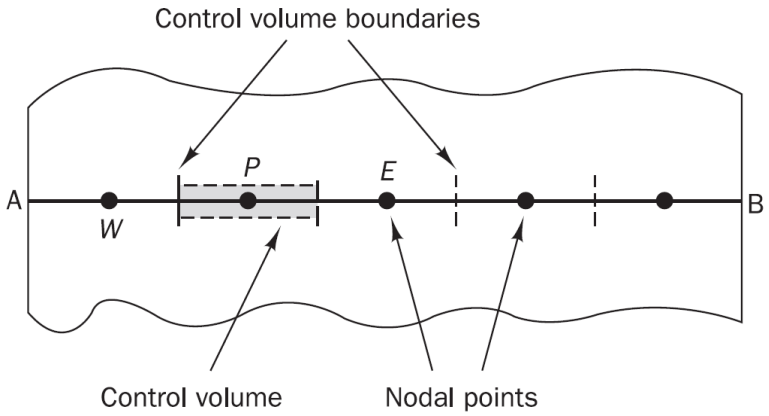

Figure 2.6 – Sketch of the line-of-sight division for the RTE integration [Versteeg and Malalasekera, 2007].

The integration of Equation 2.27 over the control volume surrounding *P* while discarding the effects from scattering and assuming constant properties and thermodynamic state at this location is:

$$\int_w^e \frac{dI_\eta}{ds} = I_\eta^e - I_\eta^w = -k_\eta^P I_\eta^P \Delta s^P + k_\eta^P I_{\eta b}^P \Delta s^P \tag{2.31}$$

where *w* and *e* are the upstream and downstream boundaries from the control volume surrounding the point of interest and Δs is the length of control volume. The superscript *P* represents the point of interest, which is exactly centered in the control volume.

Assuming a similar approach as the Upwind differencing scheme, employed in this study, it is possible to relate the intensity quantities for the *P*, *w* and *e* locations by Equations 2.32 and 2.33 respectively. The Upwind scheme uses the information of a "donor cell", i.e. the cell upstream from the point of interest and determines the value of the variable at the element face to be equal to the nodal point upstream (Versteeg; Malalasekera, 2007).

$$I_\eta^P = f I_\eta^e + (1-f) I_\eta^w \tag{2.32}$$

$$I_\eta^e = \frac{I_\eta^P - (1-f) I_\eta^w}{f} \tag{2.33}$$

where *f* is the weighting coefficient to determine the influence of the upstream cell over the current cell being calculated.

Then, one can combine Equations 2.31, 2.32 and 2.33 to determine the thermal radiation intensity at location *P*:

$$I_{\eta}^{P}=\frac{k_{\eta}^{P}I_{\eta b}^{P}\Delta s^{P}+\frac{I_{\eta}^{w}}{f}}{\frac{1}{f}+k_{\eta}^{P}\Delta s^{P}} \tag{2.34}$$

where I^{w} is given by:

$$I_{\eta}^{w}=\frac{I_{\eta}^{W}\text{-}(1\text{-}f)I_{\eta}^{ww}}{f} \tag{2.35}$$

where the superscript *ww* represent the upstream element boundary from point *W* which is one element over point *P*, hence the name.

Then, to solve the intensity field over a line of sight, Equation 2.34 must be solved for every point of the discretized control angle. The reduced form of the RTE, presented on equation, being a first order differential equation, requires that the intensity is known in at least one point of the domain. This is commonly done by either specifying the intensity of a boundary or the temperature and type of boundary (non-gray, gray, black).

With the intensity field calculated for a determined control angle, operation can be repeated over all the other control angles if the geometry being evaluated is two or three dimensional.

3. METHODOLOGY

Within this chapter, the overall procedures developed to obtain the results presented in Chapter 4 are detailed. This chapter first presents an overall description of the problem, its geometry configuration as well as the implemented boundary conditions. Then, the evaluated temperature profiles are also presented. The method for solving the RTE is presented along the evaluation of the properties of interest in this study, total hemispherical absorptivity and the benchmark reference temperature, a variable of interest that aids in the total absorptivity estimation. Finally, the mesh sensitivity study is presented, along the method of calculation of the differences between the real and estimated absorptivity and benchmark reference temperature.

3.1 STUDIED PROBLEM

The studied problem consists in the evaluation of the heat transfer by radiation between a control surface *dA,* enclosed by a black hemisphere of radius *R,* containing a participating media at atmospheric pressure (1.0 atm). This hemisphere is shown in Figure 3.1. The participating media can consist of carbon dioxide (CO_2), water vapor (H_2O) or a mixture of both, at varying mass fraction ratios. The control surface is diffuse and non-gray; therefore, its spectral emissivity is not constant over the entire spectrum. A set of temperature profiles for the participating media is evaluated, these profiles can be symmetric and asymmetric along the radial distance, *R.* The asymmetric profiles have maximum temperatures that can be close or distant to the control surface.

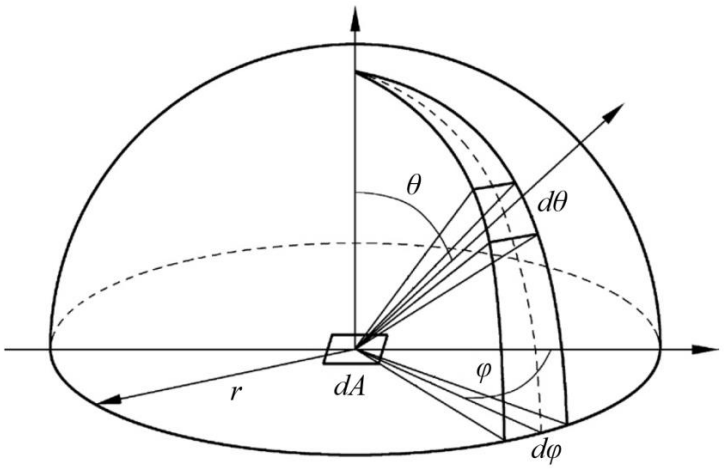

Figure 3.1 – Representation of the problem [Zhang *et al.* 2016].

The RTE is solved by the LBL integration of the spectral domain, in order to obtain the exact value for the total hemispherical absorptivity of the control surface. The spatial solution of the RTE is performed by the finite volume method (FVM), where the hemisphere is divided into a finite number of control angles, θ. Each of the control angles represent a "pencil of rays" and the radiation intensity emitted by the hemisphere, which travels across the media and is incident to the control surface is calculated. Then the intensity is integrated over all control angles.

With the spectral radiation intensity incident to the control surface, it is possible to calculate the exact total absorptivity for each individual control angle. Then this value is compared to the estimated total absorptivity. This estimation is based on specified temperatures depending on the temperature profile. Then the exact absorptivity is compared to the estimated ones verifying the error between each estimation method. Alongside it, the benchmark reference temperature, T_{reb}, is introduced in Section 3.6.5, in order to evaluate the temperature value that equates to the exact absorptivity encountered by the LBL method.

3.2 STUDIED DOMAIN

Since the boundary conditions and also the initial conditions of the problem do not present variation on the azimuthal and polar coordinates of the domain, the calculation of the hemispherical radiation over the control surface can be simplified, neglecting the influence of the φ and θ directions. Therefore, the domain variables are dependent on the radial coordinate, r, alone. A generic representation of the discretized domain can be observed on Figure 3.2, where the main geometric variables are described, noting that only a single control angle θ is needed to obtain the hemispherical solution. The hemisphere radius is constant across all of the test cases, where R=1,0 m. The spectral emissivity of the surrounding hemisphere is equal to 1, being a black surface. The control surface is modelled as diffuse and non-gray, and its spectral emissivity profile is described in Section 3.3.

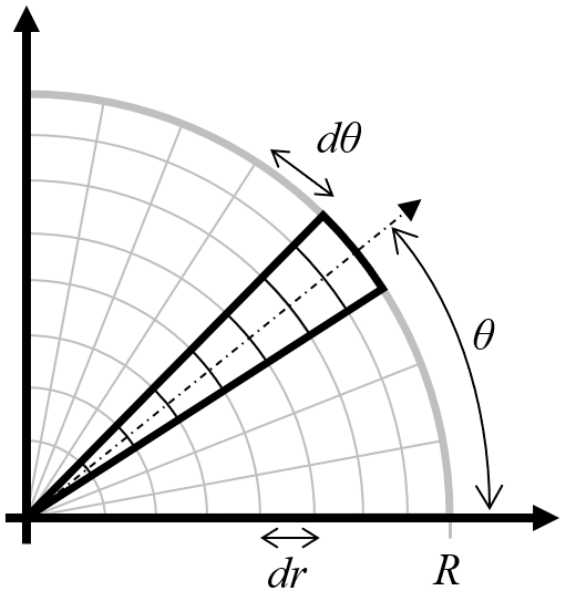

Figure 3.2 – Illustrative depiction of the evaluated geometry discretization.

3.3 BOUNDARY CONDITIONS

The calculation of the RTE requires that at least one boundary condition is specified. For the proposed problems, it is of interest the incident radiation intensity over a diffuse non-gray control surface. This radiation intensity that is emitted by a black hemisphere and travels across a participating media. The following sections describe in detail the development of said boundary conditions, and how are they implemented in the computation of the RTE in this study.

3.3.1 Surrounding Hemisphere

The boundary condition of the surrounding hemisphere using the FVM is quite straightforward, where the radiation intensity at the boundary is prescribed according to the temperature of the hemisphere. This hemisphere is considered as a diffuse and black surface; therefore, the radiation intensity emitted by it, follows the blackbody distribution, presented on Section 2.1. The intensity at the hemisphere can be obtained by Planck's law, first shown in Equation 2.1 and rewritten below in terms of wavenumber:

$$I_\eta(r=R) = \frac{2C_1\eta^3}{[exp\left(\frac{C_2\eta}{T(R)}\right) - 1]} \tag{3.1}$$

3.3.2 Control Surface

The control surface is modelled as being diffuse and non-gray. Therefore, the surface emissivity is independent on the angle of incidence of the radiation rays, but dependent on wavelength. As seen on Section 2.2, real surfaces have a irregular emissivity profiles, which would be very difficult to describe as a simple function, hence would require inputting the entire dataset on the simulation model. Another drawback is that the solution would be specific to the very surface that the data has been implemented. For this reason, the spectral properties of the surface were taken from past research papers that represent the spectral emissivity as a piecewise function of the wavelength/number.

Two spectral emissivity profiles were taken from Da Fonseca *et. al*, 2019. One of the profiles, referenced in this study as ε-Profile 1, is a piecewise function with two distinct spectral emissivity values over the entire spectrum. The emissivity values are 0.5 for the wavelength range between 0 and 4 μm and 0.9 for wavelengths above 4 μm. The second profile, which will be referenced from now on as ε-Profile 2, has multiple emissivity values over the spectrum. This profile also has an emissivity equal to 0.5 for wavelengths between 0 and 4 μm; for higher wavelengths, the emissivity has an increment of 0.1 at every 2 μm, until it reaches the value of 0.9 at 10 μm and maintain this value towards infinity. The last profile evaluated was the same one studied by Solovjov *et al*., 2013, which is representative of combustion chamber and/or flue walls covered by fly ash. This profile, called in this study as ε-Profile 3, has three distinct emissivity values. It has the emissivity value of 0.5 at the range between 0 and 4.17 μm, then the emissivity is 0.67 in the range between 4.17 μm and 5 μm. Then from 5 μm towards infinity, this profile has the emissivity of 0.93. The value for the spectral emissivity for the aforementioned profiles can be observed on Figure 3.3.

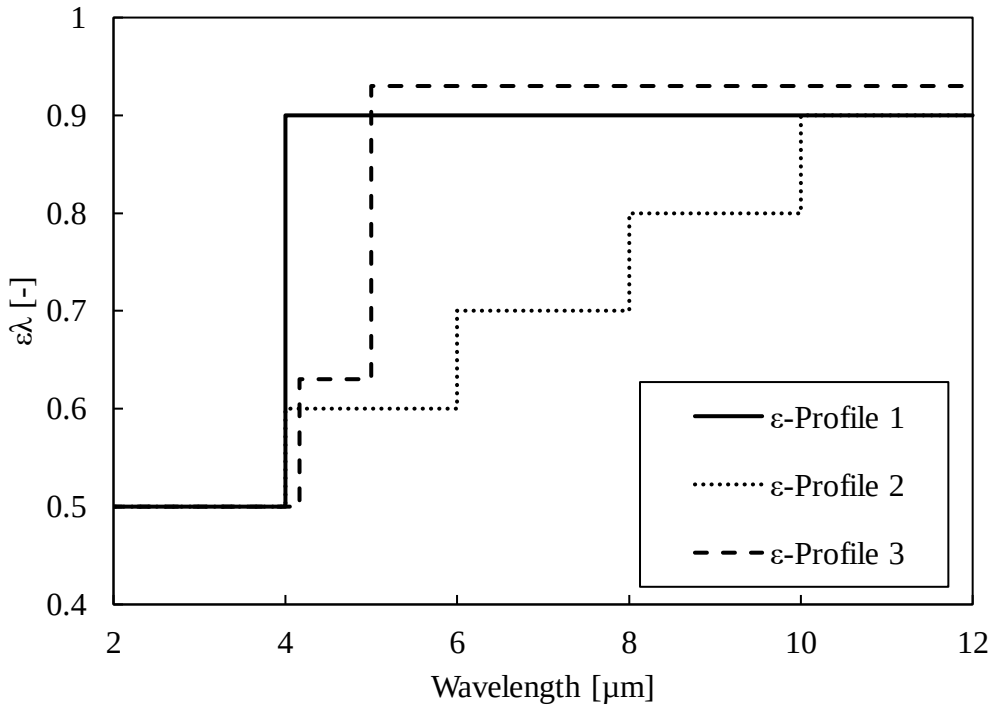

Figure 3.3 – Spectral emissivity profile of the evaluated control surface.

3.4 TEMPERATURE PROFILES

Previous studies evaluated different temperature profiles and their influence to the overall radiative heat flux and source term over the domain. In this study, some of these profiles are used to determine an estimation of the total absorptivity of the control surface of the domain, which is diffuse and non-gray. As such, a total of five temperature profiles were selected for the development of this study, considering three distinct scenarios. The first scenario is where the maximum temperature of the gas is closer to the control surface. The second is when the maximum temperature occurs at the midpoint between the control surface and the hemisphere. The third and final situation is when the maximum temperature occurs closer to the surrounding hemisphere. Three of the selected temperature profiles that match these distinct scenarios are based on the study of Fonseca et al. 2019; the other two profiles are a modification of them. The profiles used can be expressed by the following equations.

$$T(r) = (400\ K) * \left[1 + \left(\frac{10}{0,5} \right) \frac{r}{R} - \frac{5}{r^*} \left(\frac{r}{R} \right)^2 \right] \tag{3.2}$$

$$T(r)=(400\ K)*\left[1+\left(\frac{10}{0,7}\right)\left(\frac{R-r}{R}\right)-\frac{5}{(1-r^*)^2}\left(\frac{R-r}{R}\right)^2\right] \quad (3.3)$$

A total of three temperature profiles were generated by Equation 3.2, named Profile 1 when r^*=0.5, Profile 2, with r^*=0.7 and Profile 3 with r^*=0.9. Two temperature profiles were created with Equation 3.3, Profile 4, with r^*=0.3 and Profile 5 with r^*=0.1. All of these profiles are parabolic distributions and provide a large temperature gradient across the domain, with a minimum and maximum temperature of 400 K and 2400 K, respectively. Profile 1 consists of a symmetrical temperature distribution, where the maximum temperature lies at the midpoint between the control surface and the surrounding hemisphere. This profile provides the same temperature, 400 K, at both the control surface and hemisphere surface. Profile 2 provides a non-symmetrical temperature distribution, where the control surface is maintained at 400 K, the maximum temperature is shifted to r^*= 0.7, which is the non-dimensional distance between the control surface and the hemisphere radius. The hemisphere radius is maintained at 2033 K. Profile 3 have the same logic as number 2, but with the maximum temperature located at r^*= 0,9, and with a hemisphere temperature of 2375 K. Profiles 4 and 5 are mirrored versions of Profiles 2 and 3, hence their maximum temperatures occur at r^*= 0.3 and r^*= 0.1, respectively. A visual representation of the aforementioned profiles can be observed on Figure 3.4.

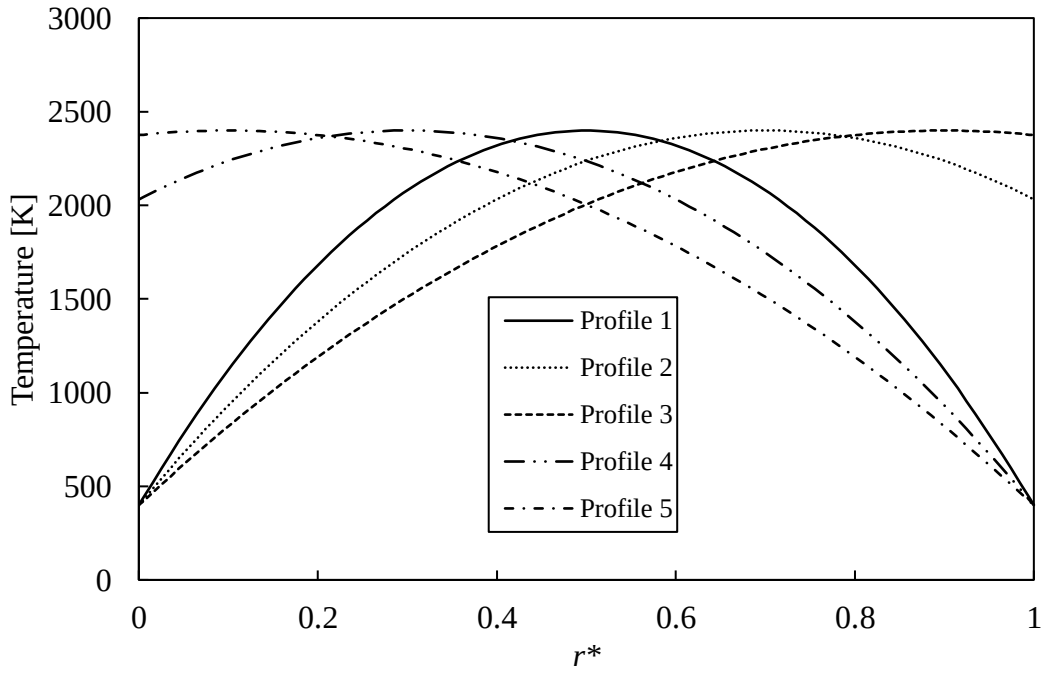

Figure 3.4 – Temperature profiles studied.

3.5 PARTICIPATING MEDIA SPECIES

The present study is focused on the thermal radiation transfer through a participating media containing mixtures of carbon dioxide, CO_2, and water vapor, H_2O. These species are common combustion products, which is the reason of their selection for this study. All of the test cases have a constant mass fraction across the domain, therefore there is no variation of concentration if these species over the radial coordinate.

In total, four different mixtures were evaluated, at different molar ratios between the species. The molar ratios studied were 2:1 for either species, at 0.1 and 0.2 molar fraction. Also, the molar ratio of 1:1, for the species was also studied at 0.1 and 0.2 for both species simultaneously. The selection of these different mixtures encompasses a wide applicable range of combustion processes, from a high to low moisture concentrations and stoichiometric ratios.

3.6 SOLUTION METHOD

The following subsections will go over the main steps that were employed in order to obtain the solution to the proposed problem. First an overview of the developed code will be given, then the method to solve the RTE spectrally and spatially is presented. Finally, the method to obtain the properties of interest is detailed.

3.6.1 FORTRAN Code

A FORTRAN code was developed in order to obtain the solution of this problem. It was based on previous studies from the LRT (Thermal Radiation Laboratory) from UFRGS, and adapted to suit the needs of the problem.

The code can be divided in four main sections. The first one is the discretization of the simulation domain, which is done according to Section 3.2. Then the boundary and initial conditions are set for the specific case that is of interest. After these two pre-processing steps, the RTE is then solved in its spectral form, by means of the finite volume method detailed in Section 2.8; this is the processing step. At the end of the processing step, with the solution ready, the properties of interest are evaluated and exported to a data file.

All of the LBL solutions, were prepared and processed on the Ubuntu Linux distribution, on its release 20.4. The workstation where the simulations were performed have a 64-bit, 6-

core Ryzen 5600X as the processor, coupled to 32Gb of physical RAM. The average simulation run time was 55 seconds per case, running in serial mode.

3.6.2 Spectral Modelling

The RTE for all of the test cases was solved spectrally using the LBL integration method, which was detailed in Section 2.7.1. The effects of scattering were not taken into account in this integration; only the effects of emission and absorption of the participating media were considered, as the medium is composed solely of H_2O and CO_2. For the LBL integration, the spectral properties for the participating media must be provided in order to perform the calculation. These properties were obtained using the HITEMP database, in its 2010 version.

The HITEMP files were generated within the spectral range from 0 to 25000 cm^{-1} at a resolution of approximately 0,067 cm^{-1}. With this configuration, a total of 375.000 spectral lines were evaluated for each case. The CO_2 database was generated only for a mass fraction of 1.0; a linear interpolation was performed for the evaluation at different values of mass fraction This was performed due to the linear behavior of the absorption coefficient for CO_2, not being affected by self-broadening (DA FONSECA, *et al.*, 2018), and is suitable for this species. On the other hand, for the H_2O, a total of four files were generated, for mass fractions of 0,01, 0,1, 0,2 and 0,4. For the intermediate mass fraction values explored in this work, a linear interpolation was also performed. All of the spectral files were obtained at a pressure of 1,0 atm, which is the same pressure evaluated in this study.

For the temperature evaluation, a set of 22 temperature nodal points were used for the spectral properties table, ranging from 400K to 2600K at regular 100K intervals. This was used in order to reduce the size of the input data required for the simulation and also reduce the processing time required for each simulation case. For the temperature, linear interpolation was also used to evaluate values between the fixed nodal points, in order to obtain the absorption coefficients at each mesh element.

3.6.3 Spatial Modelling

The spatial modelling of the RTE was performed using the finite volume method (FVM), described on Section 2.8. The discretization of the domain was performed by dividing the radial, *r*, uniformly, where a single control angle was evaluated, due to the symmetric nature of the properties on the azimuthal and polar coordinates of the hemisphere.

The solution of the RTE was done for the non-dimensional control angle, based on the emitted radiative intensity from the surrounding hemisphere, assumed black, towards the control surface. Then due to the aforementioned symmetry of the domain, no spatial integration was needed to obtain the hemispherical values, hence could be assumed the same as the directional one evaluated.

3.6.4 Absorptivity Calculation

The total absorptivity is not a property of the surface, but the result between the surface spectral absorptivity and its incident spectral radiation intensity. This makes it difficult to evaluate this property analytically, especially when the incident radiation has traveled a path across a participating media, which is the case of this study. The media has a direct impact on the amount of radiation that reaches the surface, and depending on its composition, molar concentration, temperature or pressure, can have different levels of opacity to radiation at different wavelengths. By solving the RTE trough the LBL integration, it is possible to obtain the exact value of incident intensity at the control surface, a requirement to obtain the exact total absorptivity.

The procedure to calculate the total directional absorptivity for the test cases is based on Equation 2.9, rewritten below in terms of spectral directional emissivity for a black source:

$$\alpha_{\eta,\theta} = \frac{I_{\eta,i,abs}}{I_{\eta,i}} = \frac{\int_0^\infty \varepsilon_\eta I_{\eta,b,i} d\eta}{\int_0^\infty I_{\eta,b,i} d\eta} \tag{3.4}$$

where, during the evaluation of the RTE at each individual wavenumber, the ratio between the incident and absorbed radiation is computed. After all the wavenumbers were evaluated, the solution is then integrated and the final directional absorptivity value is obtained.

The aforementioned method is related to what will be called, from now on, the LBL absorptivity, α_{LBL}. Throughout this work, new absorptivity values are also computed, based on the blackbody distribution over the spectral emissivity profile of the control surface coupled to known temperatures from the particular temperature profile of interest. By knowing the spectral emissivity distribution of the control surface, and estimating a reference temperature, the directional absorptivity can be calculated.

$$\alpha_\theta = \varepsilon_1 F_{0\rightarrow\lambda_1 T} + \varepsilon_2 F_{\lambda_1 T\rightarrow\lambda_2 T} + \ldots \tag{3.5}$$

where the subscripts for the spectral emissivity, ε, represent the spectral bands evaluated over the spectrum.

Using Equation 3.5, and taking the known temperatures from the simulated domain, four absorptivity values are calculated. The chosen temperatures were; the maximum temperature of the domain, T_{max}, the temperature of the hemisphere, T_{wall} the arithmetic average between T_{avg} and T_{wall}, called in this study as $T_{w,avg.}$ and the average domain temperature, T_{avg}, calculated by:

$$T_{avg} = \frac{\int_0^R T(r)dr}{R} \tag{3.6}$$

These temperatures provide a good baseline for comparing their effect to the resulting total absorptivity estimation, and should be effective in order to represent in an adequate manner the total absorptivity behavior for the proposed scenarios selected in this study. These temperatures should be known to the researcher, based on the temperature profiles employed, therefore can be used without the development of other arbitrary estimation.

3.6.5 Benchmark Reference Temperature

The benchmark reference temperature, or T_{reb} is a concept introduced in this work. This quantity represents the required temperature in which the total directional absorptivity calculated by means of a blackbody distribution would equate the one by the LBL solution. This was performed by executing the calculation of Equation 3.5 backwards.

However, in order to solve Equation 3.8, a temperature must be arbitrated for the calculation to be complete, since the blackbody band emission factor F is dependent on temperature. Therefore, an iterative script was written in Fortran to calculate Equation 3.8 successively until the calculated absorptivity was within 0.01% difference the exact solution (LBL). Then the temperature that complied to this convergence criteria was denominated the T_{reb} for the specific temperature profile and media composition.

Using this new reference temperature, it is possible to compare its value to the respective references detailed on the previous section, then evaluating how they fare against the LBL solution for either the temperature and total absorptivity.

3.7 MESH SENSITIVITY ANALYSIS

In order to solve the intensity field on the studied domain, an integration of the RTE must be performed spatially. In order to evaluate the influence of the spatial discretization, a mesh sensitivity analysis was conducted. This procedure consisted in the comparison between the results of the same test case when subjected to a different number of elements across the radial direction of the domain. The selected test case consisted in the combination of the temperature Profile 1, which have a symmetrical temperature distribution, alongside the ε-Profile 1, for the spectral properties of the control surface. The domain was simulated as comprised of water vapor and carbon dioxide with molar ratios of X_w=0.2 and X_c=0.1, respectively.

The mesh sensitivity was done by first testing a domain with a total of 25 elements in the radial direction of the domain, then doubling the mesh size and repeating this procedure up to a mesh of 3200 elements. Then the results for absorptivity and incident intensity at the control surface were compared, taking the finer mesh, 3200 elements, as the baseline. The results obtained for this study can be seen on Table 1.

Table 1 – Mesh sensitivity results. Temperature Profile 1, ε-Profile 1, x_c=0.1, x_w=0.2.

Mesh Size	α [-]	I [W/m²]	α Difference [%]	I_i Difference [%]
25	0.6688	158617.8	0.062	0.135
50	0.6692	158788.8	0.014	0.027
100	0.6692	158821.4	0.003	0.007
200	0.6693	158830.8	0.001	0.001
400	0.6693	158831.3	0.000	0.001
800	0.6693	158832.0	0.000	0.000
1600	0.6693	158832.1	0.000	0.000
3200	0.6693	158832.2	-	-

From the obtained results, the mesh size selected for the development of this work was the one with a total of 100 radial elements. This mesh size was selected due to the low deviation for the directional absorptivity, α and incident intensity at the control surface, I_i (less than 0.01%), and its relative low computational requirements, making it cost effective for this study.

3.8 ERROR EVALUATION

The performance of the reference temperatures discussed on Section 3.6.4, which provided the reference absorptivity values, was evaluated by means of comparing the reference absorptivity for each method to the benchmark (LBL). The deviation between these values was calculated as the following:

$$\delta_{ref} = \frac{|\alpha_{ref} - \alpha_{LBL}|}{\alpha_{LBL}} \; 100\% \tag{3.7}$$

where the *ref* subscript represents the reference method for the absorptivity calculation.

3.9 SUMMARY OF TEST CASES

In the previous subsections it was discussed each individual points of interest that were evaluated in this study. These were the different temperature profiles used, the concentration of the species evaluated in the simulation domain and also the spectral properties of the control surface. To organize and name all of the test cases that shall be presented in the next chapter, Table 2 was created. A total of 60 test cases will be presented, comprising 5 temperature profiles, 3 spectral emissivity distributions for the control surface and 4 different molar fractions for the mixture of CO_2 and H_2O.

Table 2 – Summary of test cases for the present study.

Test Case	Temperature	Surface Properties	X_c	X_w	Test Case	Temperature	Surface Properties	X_c	X_w
1a	Profile 1	ε-Profile 1	0.1	0.2	1c	Profile 1	ε-Profile 1	0.1	0.1
2a	Profile 2				2c	Profile 2			
3a	Profile 3				3c	Profile 3			
4a	Profile 4				4c	Profile 4			
5a	Profile 5				5c	Profile 5			
6a	Profile 1	ε-Profile 2			6c	Profile 1	ε-Profile 2		
7a	Profile 2				7c	Profile 2			
8a	Profile 3				8c	Profile 3			
9a	Profile 4				9c	Profile 4			
10a	Profile 5				10c	Profile 5			
11a	Profile 1	ε-Profile 3			11c	Profile 1	ε-Profile 3		
12a	Profile 2				12c	Profile 2			

13a	Profile 3				13c	Profile 3			
14a	Profile 4				14c	Profile 4			
15a	Profile 5				15c	Profile 5			
1b	Profile 1				1d	Profile 1			
2b	Profile 2	ε-Profile 1			2d	Profile 2	ε-Profile 1		
3b	Profile 3				3d	Profile 3			
4b	Profile 4				4d	Profile 4			
5b	Profile 5				5d	Profile 5			
6b	Profile 1				6d	Profile 1			
7b	Profile 2	ε-Profile 2	0.2	0.1	7d	Profile 2	ε-Profile 2	0.2	0.2
8b	Profile 3				8d	Profile 3			
9b	Profile 4				9d	Profile 4			
10b	Profile 5				10d	Profile 5			
11b	Profile 1				11d	Profile 1			
12b	Profile 2	ε-Profile 3			12d	Profile 2	ε-Profile 3		
13b	Profile 3				13d	Profile 3			
14b	Profile 4				14d	Profile 4			
15b	Profile 5				15d	Profile 5			

4. RESULTS AND DISCUSSION

In this section, the results obtained by following the methodology described in Chapter 3 are presented. This chapter is divided in three main sections. The first one will consider the symmetrical temperature profile, Profile 1. Then the results for the asymmetrical temperature profiles where the maximum temperature is close to the hemisphere border, Profile 2 and 3, are presented. Finally, in the final section the asymmetrical temperature profiles with their maximum temperatures closest to the control surface are shown, that is, for Profile 4 and 5. For each temperature profile, different molar fractions of water vapor and carbon dioxide were tested, alongside different spectral profiles for the control surface.

4.1 SYMMETRICAL TEMPERATURE PROFILE

This section comprises the results obtained for the temperature Profile 1, given by Equation 3.2. This profile has a symmetrical temperature distribution, where the control surface and the hemisphere border are at the same temperature. The maximum temperature for this profile is at the midpoint of the domain, as it was shown in Figure 3.4.

The results are organized for each spectral emissivity profiles, called ε-Profiles, to distinguish them from the temperature ones. For each of these ε-Profiles, plots for the total absorptivity, α, as well as the benchmark reference temperature, T_{reb}, are shown. These values are then compared to the reference methodologies described on Sections 3.6.4 and 3.6.5.

4.1.1 ε-Profile 1

The four test cases comprising the symmetrical temperature profile, as well as the ε-Profile 1 are evaluated in this section. The four cases, with different concentrations of the participating species were simulated; the results for the total absorptivity and benchmark reference temperature are shown in Figure 4.1(a) and Figure 4.1(b), respectively. In Figure 4.1(a), the absorptivity of the surface calculated by the LBL integration method is shown by the plot markers, with the circle and square representing the test cases with a CO_2 molar fraction of 0.1 and 0.2 respectively. The plots are a function of absorptivity and H_2O concentration, in order to show the influence of the varying concentration of the species to the total absorptivity. The LBL absorptivity, which is the benchmark solution, is then compared to absorptivity values calculated according Section 3.6.4 for different temperatures of the domain. The temperature

called T_{avg} corresponds to the average temperature of the participating species that are present in the simulation domain. The one named T_{wall} is the temperature at which the black hemisphere border is at, which is the main source of radiation intensity. T_{max} is the maximum temperature of the participating species and $T_{w,avg}$ is the arithmetic average between T_{avg} and $T_{wall.}$ The image showing T_{reb}, on Figure 4.1(b), plots alongside it the aforementioned temperatures. This is useful to check what is the reference temperature method that more closely matches the temperature that would provide the LBL absorptivity value.

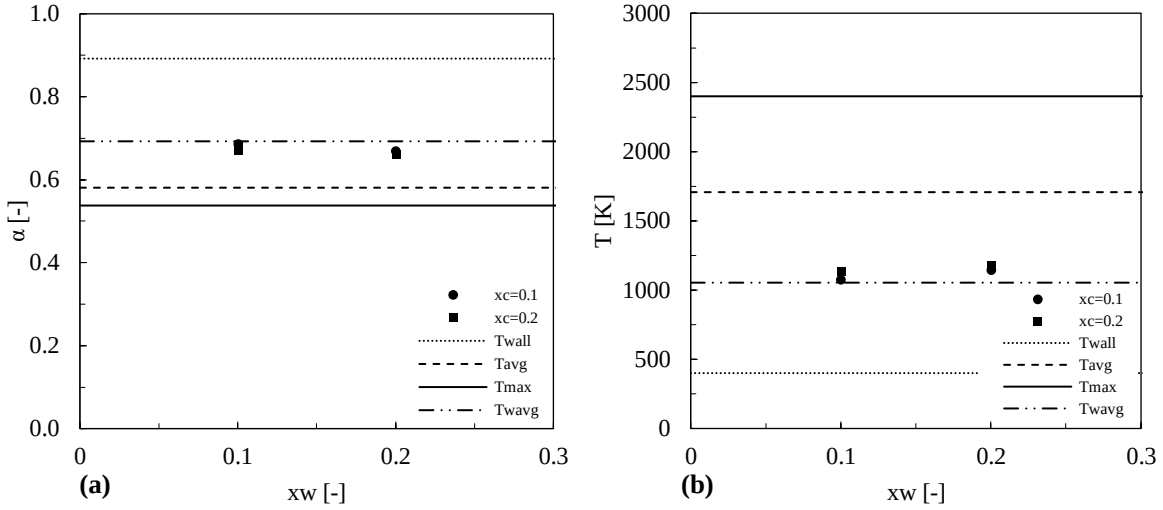

Figure 4.1 – Total absorptivity (a) and benchmark reference temperature (b) for the Profile 1 and ε-Profile 1 at different concentrations of CO_2 and H_2O.

From the results presented on Figure 4.1(a), the LBL absorptivity value for the four test cases was very similar despite the different molar fraction and molar ratios between the species. The LBL absorptivity values ranged from 0.661 to 0.686, for molar ratios of X_c=0.2, X_w=0.2 and X_c=0.1, X_w=0.2, respectively, which is a relatively small variation. When comparing the LBL absorptivity values with the ones calculated by the reference methodologies, it is clear that for this combination on temperature and spectral emissivity profiles, utilizing the reference temperature $T_{w,avg}$ provides the closest results to this benchmark, followed by using T_{avg} as a reference. Calculating the absorptivity by $T_{w,avg}$, the values achieved the lowest deviations to the LBL solution, with a minimum deviation between the test cases of 0.9% and a maximum of 4.8% for the molar ratios of X_c=0.1, X_w=0.1 and X_c=0.2, X_w=0.2, respectively. One can also observe that with the increase of the molar concentration of either carbon dioxide ans water vapor, the LBL absorptivity reduces, with the tendency to approach the values obtained by using T_{avg} as the reference. This also indicates a stronger influence on the emittance of the

medium, since with an increase of molar fraction, the participating media becomes more opaque to the radiation emitted by the hemisphere. Hence the domain has a strong influence over the emitted radiation intensity that is incident to the control surface.

The results presented on Figure 4.1(b) corroborate the aforementioned observations, where the value for $T_{w,avg}$ of this temperature profile, is the closest match to the benchmark reference temperature, T_{reb}, obtained by the methodology discussed in Section 3.6.5. The value of T_{reb} varies for different molar fractions of the species, but similarly of what occurs for the absorptivity values, they do not show a significant variation. When comparing this benchmark reference temperature to the proposed calculation methodologies, $T_{w,avg}$ showed the smallest deviation from the T_{reb} at 2.2% for a molar fraction of X_c=0.1, X_w=0.1. This deviation increases to 10.9% when the molar concentration for both of the species is doubled. From the results, it is clear that in this configuration, the least effective methodology is to assume the wall temperature, T_{wall} as the reference. This temperature achieved the highest deviations from T_{reb}, with an error of 62.9%. Therefore, for these temperature and spectral emissivity profiles, this reference temperature is not recommended, since it would produce significant errors to the amount of radiation energy that is absorbed and hence reflected by the surface.

It is important to note that, when comparing the absorptivity deviations to the ones encountered for the reference temperatures, they are significantly smaller for the absorptivity values. Therefore, even if the deviation of the reference temperature to T_{reb} is large, this would not mean that the value for the absorptivity would be as expressive. This is the case for all references, such as the maximum deviation of T_{wall} is 62.9% as mentioned earlier. When calculating its reference total absorptivity value, this resulted in a deviation of 30.0%. While estimating the absorptivity by $T_{max,}$ the temperature deviation reaches 122.7% and still achieves a smaller absorptivity deviation, at 21.6%. This is the case due to the larger difference between the values of T_{reb} and the reference temperatures, which can differ from hundreds of Kelvin, while the absorptivity range only exists between 0 and 1.

4.1.2 ε-Profile 2

The same temperature profile and molar concentration of the participating species was also tested with a different spectral emissivity profile of the control surface, ε-Profile 2. This profile has a gradual increase of intensity over the wavelengths, with a total of five distinct steps, as shown in Figure 3.3.

The results for the total absorptivity obtained by the LBL method, represented by the markers are compared to the total absorptivity calculated by the reference temperatures on Figure 4.2(a), represented by the various lines on the plots. A similar plot, comparing the benchmark reference temperature for the four molar concentration test cases are compared to the reference temperatures, on Figure 4.2(b).

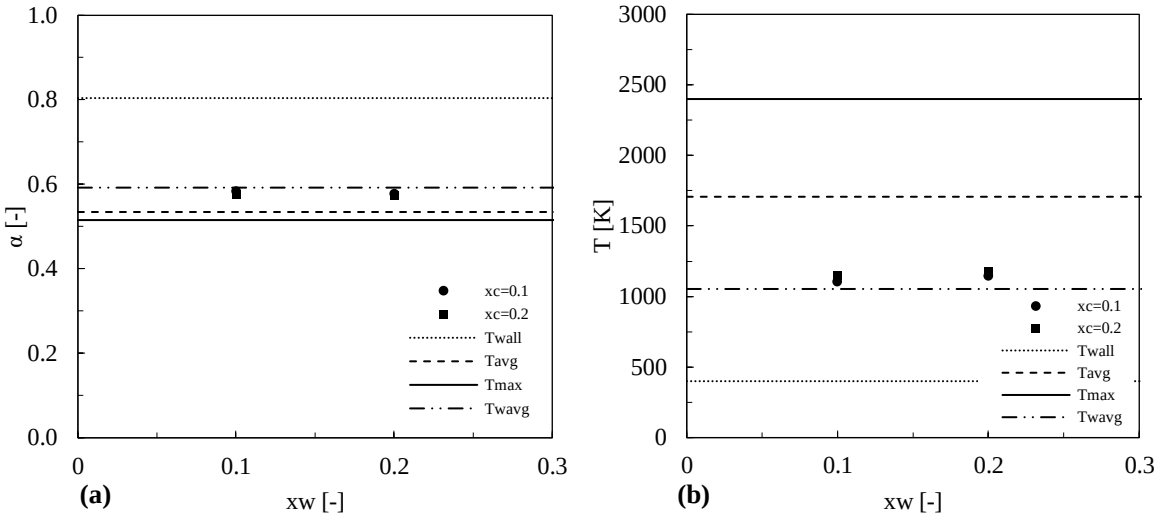

Figure 4.2 – Total absorptivity (a) and benchmark reference temperature (b) for the Profile 1 and ε-Profile 2 at different concentrations of CO_2 and H_2O.

By observing the total absorptivity for the four test cases presented in Figure 4.2(a), it is possible to verify their close proximity to the absorptivity calculated by utilizing $T_{w,avg}$ as the reference. For a molar ratio of 1.0, the absorptivity values ranged from 0.575 and 0.584 when the molar concentration of the participating species were 0.1 and 0.2, respectively. This showed a slight increase in the absorptivity value with a domain with higher concentration of gases that are opaque to thermal radiation. For a molar ratio of 2.0, either for CO_2 and H_2O, the absorptivity values were similar, reaching 0.578 and 0.579, respectively. The absorptivity obtained by using $T_{w,avg}$ as a reference attained a value of 0.592, thus when comparing to the LBL absorptivity, this method achieved a maximum deviation of 3% and a minimum of 1.3%. With the increase of the optical thickness of the medium, i.e., the increase of the concentration of the species, the deviation increased for the $T_{w,avg}$ reference. The use of T_{wall} as a reference achieved deviations of up to 8.6%, for molar concentrations of X_c=0.1, X_w=0.1 and a deviation of 7.1% for concentrations of X_c=0.2, X_w=0.2. For these test cases, the least effective reference temperatures for the absorptivity estimation are the maximum temperature, T_{max} and the wall

temperature, T_{wall}. These reference temperatures achieved the largest deviations for the test cases, reaching the values of 21.6% and 35% respectively.

When comparing the reference temperatures to T_{reb}, the exact reference temperature, the one that provided the closest match was the arithmetic average between the wall temperature and the average temperature of the domain, $T_{w,avg}$, represented by the dot-dashed line in Figure 4.2(b). The reference temperature for the evaluated test cases increased with the increase of molar concentration of the species, moving towards the dashed line, which represent the average domain temperature, T_{avg}. Again, this corresponds to a stronger influence of the participating species temperatures with optically thick media. The maximum deviations of $T_{w,avg}$ and T_{avg} when compared to T_{reb} are 10.4% and 54.5%, respectively, accounting for smaller deviations on the absorptivity values, 8.6% and 3%, the values mentioned earlier. Therefore, despite the expressive deviation of the reference temperatures, these values do not correspond to such higher deviations in the calculated absorptivity values, as previously mentioned.

4.1.3 ε-Profile 3

Following the evaluation of the test cases for the symmetrical temperature profile, the absorptivity values and the benchmark reference temperatures were obtained for the spectral emissivity profile of the control surface called ε-Profile 3. This profile was obtained by experimental testing and used in non-gray wall simulations in the literature. It represents a surface coated in fly ash, as was stated in Section 3.3.2.

The results are presented in similar fashion as for the previous ε-Profiles. On Figure 4.3(a), the total absorptivity value for the test cases, obtained by the LBL integration of the RTE over the participating media domain is compared against the absorptivity values obtained by the reference temperature methodology. The absorptivity values are plotted on the abscissa, and the ordinates axis represents the variation in water vapor molar concentration. While on Figure 4.3(b), the value for T_{reb} for the testcases is compared to the reference temperatures for this temperature profile, in the same manner, with the ordinate axis representing the water vapor molar concentration, with different marker types indicating the different molar concentration of carbon dioxide and on the abscissa the temperatures are given.

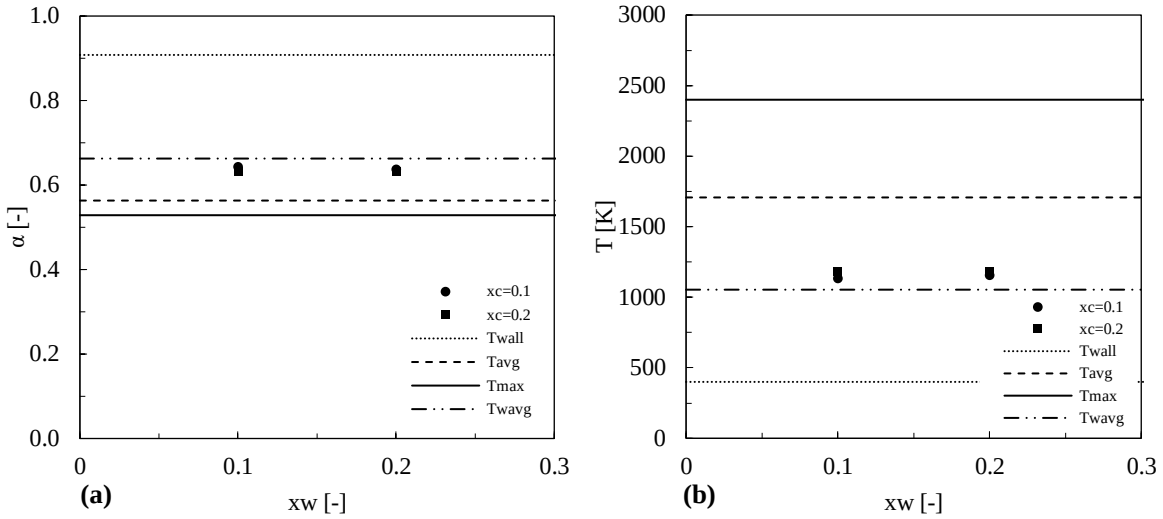

Figure 4.3 – Total absorptivity (a) and benchmark reference temperature (b) for the Profile 1 and ε-Profile 3 at different concentrations of CO_2 and H_2O.

This profile achieved similar results as the ones discussed previously, with a closer resemblance to the ε-Profile 1. Both emissivity profiles have similar values and transition points for their emissivity values over the spectrum, but ε-Profile 3, has an additional spectral emissivity step, between 4.16 μm and 5 μm. The absorptivity encountered for the test cases comprising the temperature Profile 1 and the ε-Profile 3 ranged from 0.632 and 0.643 for the case with X_c=0.2;X_w=0.2 and X_c=0.1;X_w=0.1, respectively. With this profile, the absorptivity value presented the behavior of reducing its value with the increase of the optical thickness of the medium. Also showed little variation in its magnitude for the different molar concentrations of the medium, being quite stable within the studied range, which matches usual concentration of combustion products. The reference absorptivity that gave the best results was again the one based on $T_{w,avg}$, providing the smallest deviation of the testcases when comparing against the exact solution (LBL integration), at 3.1% for X_c=0.1;X_w=0.1. This deviation increased when using this reference for a thicker optical medium, reaching 4.9% for X_c=0.2;X_w=0.2. For this combination of temperature and surface emissivity profiles, the least favorable reference temperature was T_{wall}, achieving the highest deviation from the results presented so far, at 43.7% for a medium with a molar fraction of CO_2 and H_2O of 0.2.

When observing the benchmark reference temperature at Figure 4.3(b), the value obtained for the evaluated simulations achieved values that were close to the estimation given by $T_{w,avg.}$ This is corroborated with the comparison of the absorptivity values given in the previous paragraph. The values for T_{reb} for these simulated cases ranged from 1137K and 1188K, while the value for $T_{w,avg}$ for this temperature profile was 1053K. This represented a maximum

deviation from the benchmark reference temperature of 11.4%, which resulted in an error in 4.9% in the absorptivity value, for the case with X_c=0.2;X_w=0.2.

From the results obtained for a symmetrical temperature profile, established by Profile 1, and presented in the current section, despite the differences the surface properties and domain concentrations, for the 12 cases evaluated, all of them provide absorptivity values that could be better estimated using the reference temperature based on the arithmetic average between the hemisphere border temperature and the average temperature of the participating species, $T_{w,avg}$. This reference provided an average deviation from the LBL total absorptivity of 3.2% over the 12 cases evaluated for this scenario, and a maximum deviation of only 4.9% in one of the test cases. The second-best reference that could represent the absorptivity value was T_{avg}, with an average deviation of 10.9%. The other references could not provide an adequate representation of the total absorptivity for the surfaces, due to their high deviations, 15.9% for T_{max} and 38.1% for T_{wall}, at an average. The summary of the results for the absorptivity values obtained by the LBL integration and the reference temperature methodologies, along with their deviations, can be seen on Table 3.

Table 3 – Summary of results for the symmetrical temperature profile, Profile 1.

ε-Profile	X_c [-]	X_w [-]	T_{reb} [K]	α_{LBL} [-]	δT_{avg} [-]	δT_{wall} [-]	δT_{max} [-]	$\delta T_{w,avg}$ [-]
ε-1	0.1	0.1	1077.8	0.686	15.4%	30.0%	21.6%	0.9%
	0.1	0.2	1146.0	0.669	13.2%	33.3%	19.6%	3.5%
	0.2	0.1	1137.4	0.671	13.5%	32.9%	19.9%	3.2%
	0.2	0.2	1182.6	0.661	12.1%	35.0%	18.6%	4.8%
ε-2	0.1	0.1	1105.2	0.584	8.6%	37.6%	11.8%	1.3%
	0.1	0.2	1147.3	0.579	7.7%	38.9%	10.9%	2.3%
	0.2	0.1	1149.5	0.578	7.6%	39.0%	10.9%	2.4%
	0.2	0.2	1176.0	0.575	7.1%	39.8%	10.4%	3.0%
ε-3	0.1	0.1	1137.0	0.643	12.4%	41.3%	17.8%	3.1%
	0.1	0.2	1159.1	0.638	11.7%	42.3%	17.1%	3.9%
	0.2	0.1	1186.3	0.632	10.9%	43.6%	16.4%	4.8%
	0.2	0.2	1188.8	0.632	10.8%	43.7%	16.3%	4.9%

4.2 ASYMMETRICAL TEMPERATURE PROFILES – MAXIMUM FAR FROM CONTROL SURFACE

The evaluation of the absorptivity of diffuse non gray surface enclosed by a black hemisphere filled with a mixture of non-transparent media continues in this section, but now with asymmetrical temperature distributions over the domain. This specific section evaluates

temperature Profiles 2 and 3. These profiles are defined by Equations 3.3 and 3.4, and have the maximum temperature occurring closer to the hemisphere border. This also means that the temperature at the hemisphere is also greater, than it was for the Profile 1, shown in the previous section. Profiles 3 and 4 have respectively, T_{wall} equal to 2032.6 K and 2375.3 K, T_{avg} equal to 1883 K and 1791 K, $T_{w,avg}$ equal to 1958 K and 2083 K. Their maximum temperatures, T_{max} are the same, at 2400 K. The evaluation of these profiles will follow the same methodology and organization as the previous section.

4.2.1 ε-Profile 1

For the ε-Profile 1, first are shown the results for the temperature Profile 2, with the maximum temperature located at a unidimensional radius equal to r^*=0.7. The same four testcases were simulated, with different molar concentration of the species, CO_2 and H_2O. The value for the absorptivity calculated via the LBL integration of the RTE is plotted against the absorptivity calculated by the reference temperature method, for different temperatures, on Figure 4.4(a), while the benchmark reference temperatures for these absorptivity values are plotted on Figure 4.4(b).

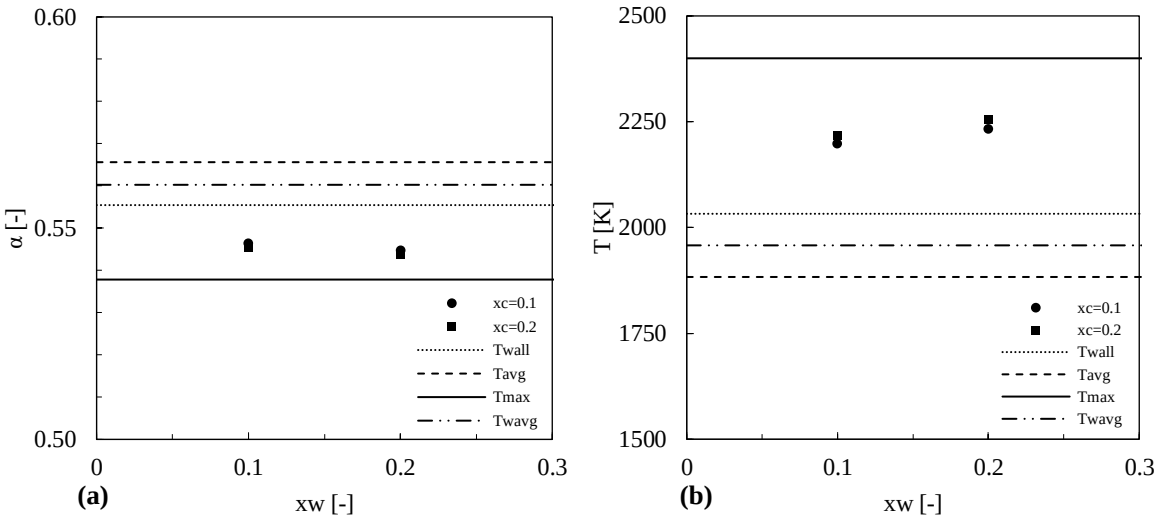

Figure 4.4 – Total absorptivity (a) and benchmark reference temperature (b) for the Profile 2 and ε-Profile 1 at different concentrations of CO_2 and H_2O.

The results found for the combination of temperature Profile 2 and spectral emissivity of the surface, ε-Profile 1, provided a much narrower range for the absorptivity, with minimal variation within the molar concentration of the species evaluated, when compared to the results

with the symmetrical temperature profile. This can be linked to the higher average temperature of the domain and hemisphere, weighing the absorptivity towards a lower value, close to 0.5. The absorptivity went from a value of 0.546 for the case where X_c=0.1;X_w=0.1 to 0.544 for X_c=0.2;X_w=0.2. This showed a slight decrease in the absorptivity value with the increase of concentration of participating media in the domain. Comparing the LBL absorptivity values against the ones calculated by the reference temperatures, the ones that provided the best estimation was the use of T_{max} with a minimum deviation to the exact results of 1.1% and a maximum of 1.6%. The use of T_{wall} as a reference also provided good results, with a minimum and maximum deviation to the exact results of 1.7% and 2.1%, respectively. The use of the values of T_{avg} and $T_{w,avg}$ also provided satisfactory results, with an average deviation to the exact results of 3.8% and 2.8%, respectively.

When evaluating the benchmark reference temperature, T_{reb}, plotted against the references from the temperature profile on Figure 4.4(b), it lies close to the midpoint between T_{wall}, shown in the dotted line, and T_{max}, shown in the continuous line. The results, similarly to what happened to the symmetrical temperature profile, shown that even with a high deviation to the reference temperature, the deviation to the absorptivity value did not achieve such higher values. This can be linked to the unlimited range of possible values for $T_{reb,}$, compared to the narrow range of absorptivity, only existing between 0 and 1. With T_{max}, the average deviation from the test cases was 7.8% for the temperature, while this achieved the average absorptivity deviation of 1.3%. This occurred also for the use of T_{wall}, with a temperature deviation to T_{reb} of 8.7% the resulting absorptivity deviation was 1.9%.

Temperature Profile 3 is also evaluated in this section, alongside ε-Profile 1. This temperature distribution over the domain, described by Equation 3.4, achieves a maximum temperature value at the position r^*=0.9. With this, the black hemisphere that is emitting the radiation over the control surface has a major role, due to its higher temperature, when compared to the participating media temperature. The results for the obtained absorptivity values for the test cases is plotted on Figure 4.5(a), while the benchmark reference temperature is plotted on Figure 4.5(b).

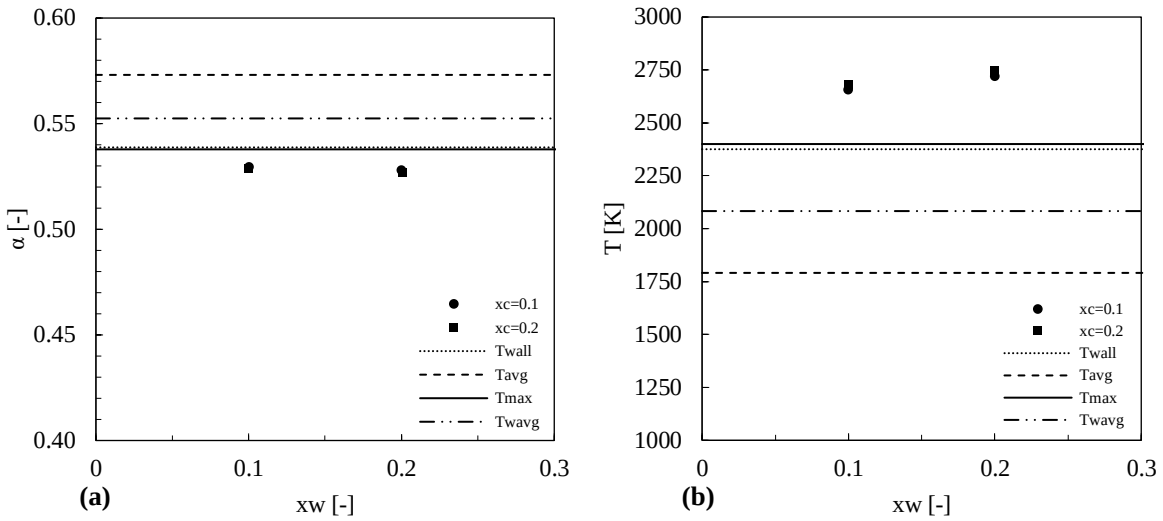

Figure 4.5 – Total absorptivity (a) and benchmark reference temperature (b) for the Profile 3 and ε-Profile 1 at different concentrations of CO_2 and H_2O.

With the values for the absorptivity in different molar concentration of the participating media, it is possible to once again verify that for a practical range of these species, there is little variation on the exact absorptivity of a surface described by the ε-Profile 1. The absorptivity values lay in the range between 0.527 and 0.530, and these extremes correspond to the thicker and thinner optical paths, X_c=0.2;X_w=0.2 and X_c=0.1;X_w=0.1, respectively.

Comparing the absorptivity values, one can note that the values obtained by the exact solution (LBL integration) are lower than all of the values calculated by the reference methodology. This would suggest that the absorptivity is referenced to a higher temperature than the ones used as a reference, since the blackbody maximum spectral intensity shifts towards smaller wavelengths. With this, more energy is emitted at the position in the spectrum where the spectral emissivity of the surface has a lower value, increasing its "weight" over the other portions of the spectrum. This is corroborated by the results presented in Figure 4.5(b), which demonstrated that the value for T_{reb} is higher than even the maximum temperature of the domain. This could be linked to the emissivity properties of the surface of interest mathching with the participating media higher spectral emission at a given position of the spectrum. Due to the spectral dependence of the participating media, some wavelengths could be attenuated and others emitted along the radiation ray path. These variations in the "packets" of energy that reaches the control surface can shift the resulting absorptivity value to one that would represent a temperature even higher than the domain maximum, since the reference temperature methodology assumes the absorptivity calculation from the blackbody distribution.

Despite these variations, the results provided that the most adequate estimate for the real absorptivity is the one using the maximum temperature of the domain, alongside with the use of the hemisphere temperature, T_{max} and T_{wall}, respectively. The average deviation of the absorptivity values from the four test cases was 0.6% when using T_{max} and 0.7 when using T_{wall} as the reference temperature methodology.

4.2.2 ε-Profile 2

The surface emissivity profile with five distinct steps over the wavelength is evaluated in this section, for the asymmetrical temperature profiles where the maximum value is located closest to the hemisphere border. We start evaluating the results for the temperature Profile 2. The resulting absorptivity values for the four different species concentrations are shown on Figure 4.6(a), where the LBL values are plotted with markers at the specific molar concentration of water vapor in the mixture, while the lines represent the absorptivity calculated by the reference methodologies. Figure 4.6(b) shows the reference temperatures of the test cases in a similar manner, where the value for T_{reb} is plotted on the figure as markers, while the reference temperature used are represented by lines.

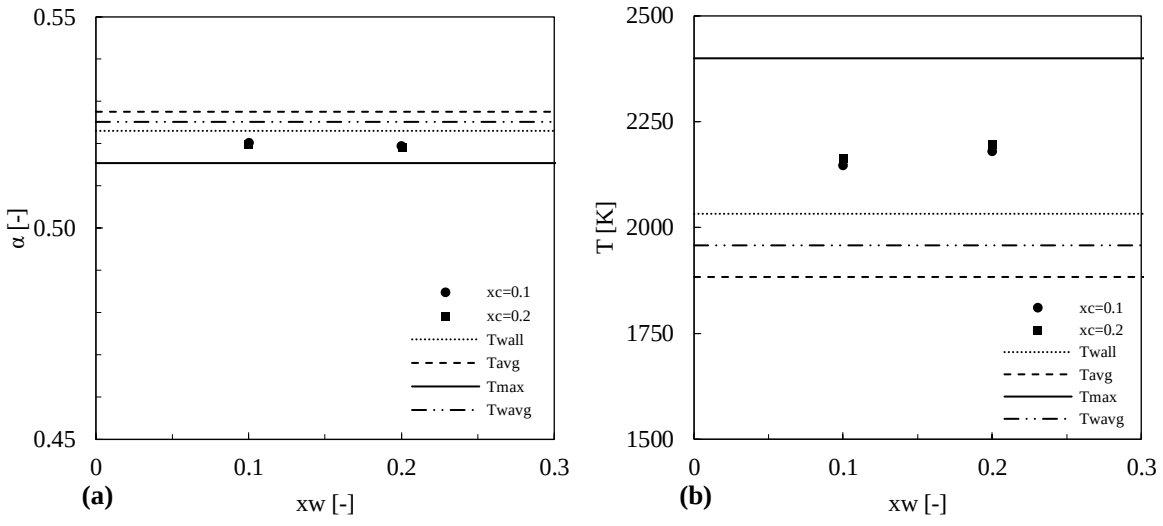

Figure 4.6 – Total absorptivity (a) and benchmark reference temperature (b) for the Profile 2 and ε-Profile 2 at different concentrations of CO_2 and H_2O.

By the results obtained with the combination of temperature Profile 2 and ε-Profile 2, it is possible to observe that despite the various molar concentrations of the species, there was almost no variation in the total absorptivity value, ranging from 0.519 to 0.520 for the cases

with X_c=0.2;X_w=0.2 and X_c=0.1;X_w=0.1, respectively. This was a common observation from all of the testcases evaluated. Also, comparing these absorptivity values, which were calculated by integrating the RTE over the spectrum, to the reference methodologies, they are located between the values obtained by the T_{max} and T_{wall} references. These references provided a good agreement with the exact solution, reaching maximum deviations of only 0.9% and 0.8%, respectively. The average deviation over the four testcases presented on Figure 4.6(a) for T_{max} and T_{wall} as references were 0.8% and 0.6%, therefore cementing them as excellent reference temperatures to be used with this profile combination.

When evaluating the reference temperatures, the T_{reb} value obtained for the test cases complied to the comments made on the previous paragraph, where they lied on between the reference temperatures of T_{max} and T_{wall}. Similarly, to what occurred on previous evaluations, the deviation of T_{reb} to the reference temperatures achieved greater deviations than the ones for the reference absorptivity. T_{max} and T_{wall} achieved a maximum deviation to T_{reb} of 11.8% and 7.4%, and an average deviation of 10.6% and 6.4%, respectively. Therefore, despite the large deviation on the benchmark reference temperature, these methodologies still provided a good agreement to their respective absorptivity results.

Moving to temperature Profile 3, the results for the absorptivity presented in Figure 4.7(a) and the benchmark reference temperature, in Figure 4.7(b), the results showed a similar overall behavior to the previous emissivity profile.

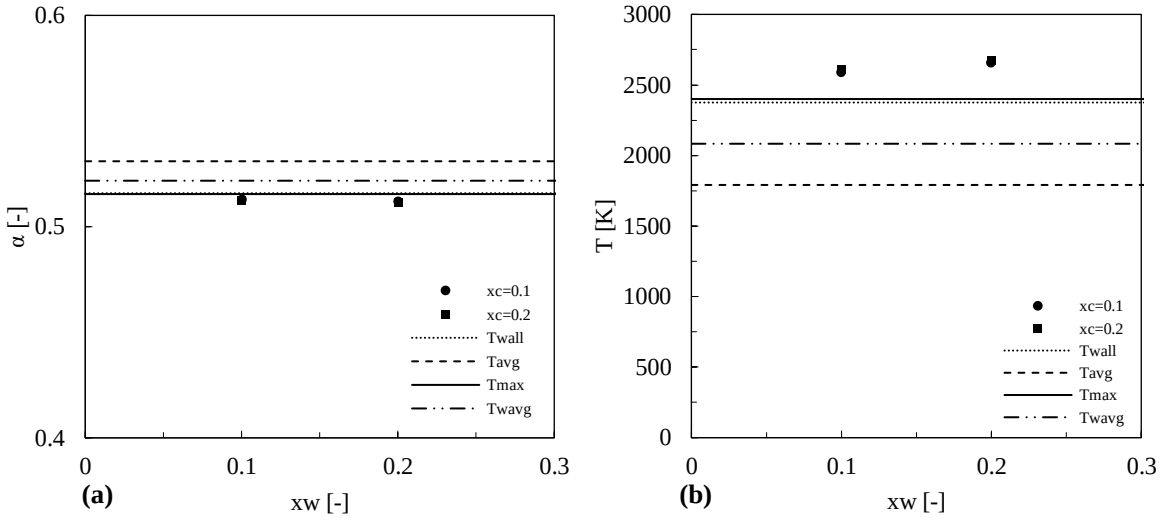

Figure 4.7 – Total absorptivity (a) and benchmark reference temperature (b) for the Profile 3 and ε-Profile 2 at different concentrations of CO_2 and H_2O.

The absorptivity values attained little to no variation with the various molar concentration of the species testes, ranging from 0.512 to 0.513 for X_c=0.2;X_w=0.2 and X_c=0.1;X_w=0.1, respectively. Again, for this temperature profile, the reference that provided the best agreement with the LBL solution was T_{max}, closely followed by T_{wall}. The average deviation for the absorptivity value using T_{max} as the reference was 0.6%, and using T_{wall} was 0.7%, which represent very good approximations of the real absorptivity value. However, in this temperature range, all of the references employed achieved average deviations over the test cases below 4%. The use of $T_{w,avg}$ and T_{avg} provided an average deviation of 1.9% and 3.7%, respectively. This could be linked to the high temperatures of the domain, that shift the absorptivity values toward smaller values, close to the lower limit of the ε-Profile 2, which is being evaluated.

The benchmark reference temperatures for the test cases with the temperature Profile 3 were found to be higher than the maximum temperature of the domain. This is again linked to the spectral dependence of the participating media, which shifted the absorptivity to a lower value. This lower absorptivity then is better represented with a higher temperature, by calculating it through a blackbody spectral distribution, which the reference methodology utilizes. The value for T_{reb} for the test cases ranged from 2590.8K to 2679.8K, for X_c=0.1;X_w=0.1 and X_c=0.2;X_w=0.2, respectively. This corresponded to a deviation of 7.7% and 10.4% when using T_{max} as a reference, and 8.3% and 11.4% when using $T_{wall.}$

4.2.3 ε-Profile 3

The ε-Profile 3, representing the spectral emissivity of a surface coated with fly ash is evaluated over the same molar concentration of the participating species as the previous evaluations. When this surface is subjected to the incident radiation that travelled a domain represented by the temperature Profile 2, the resulting total absorptivity of the surface is plotted on Figure 4.8(a), while the benchmark reference temperature is plotted on Figure 4.8(b).

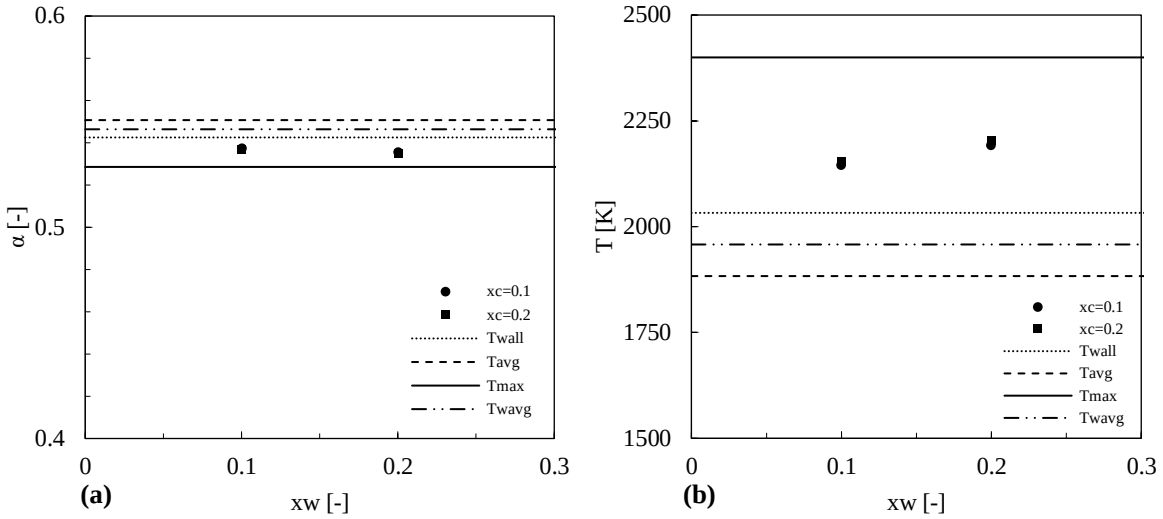

Figure 4.8 – Total absorptivity (a) and benchmark reference temperature (b) for the Profile 2 and ε-Profile 3 at different concentrations of CO_2 and H_2O.

The absorptivity of a surface represented by the ε-Profile 3, as shown on Figure 4.8(a), did not present an expressive variation in its value for the different concentrations of the participating media. Being the optical thickness small, with X_c=0.1;X_w=0.1, the absorptivity calculated by the LBL integration of the RTE, which is the benchmark solution, achieved a value of 0.537, while with a thicker medium, where X_c=0.2;X_w=0.2, the absorptivity value dropped only 0.002 units, reaching a value of 0.535. For this combination of temperature and emissivity profiles, the references that provided the best agreement to the exact absorptivity were the ones based on the maximum domain temperature, T_{max} and on the hemisphere wall temperature, T_{wall}. The use of maximum temperature achieved a small deviation to the exact result, with an average between the cases of 1.4%, while the use of the hemisphere wall temperature provided even better representation of the surface, with an average deviation of only 1.2%.

The benchmark reference temperature also corroborated with the findings described above, with the average value of T_{reb} for the four test cases presented on Figure 4.8(b) equal to 2175K, it is located close to the midpoint between T_{wall} and T_{max}, at 2032.6K and 2400K respectively. This showed that either of these references could provide adequate estimations for the total absorptivity of a surface represented by the ε-Profile 3, alongside a temperature distribution corresponding Profile 2.

The results for the temperature Profile 3, where the absorptivity values are plotted on Figure 4.9(a) and the benchmark reference temperatures on Figure 4.9(b), shown a similar behavior for this ε-Profile and the previous ones. The absorptivity did not show a significant

modification with the different molar ratios and concentration of the participating media mixture and the absorptivity calculated via T_{wall} and T_{max} provided the best agreement with the exact values. The absorptivity value ranged from 0.521 at its lowest value and 0.524 at it highest. These values correspond to the test cases where X_c=0.2;X_w=0.2 and X_c=0.1;X_w=0.1 were the mixture of the participating gases, respectively. From all of the four test cases, the reference temperature that provided the best overall accuracy to represent the real absorptivity of the control surface, was T_{max}, at an average deviation of 1.1% of the exact value, followed closely by T_{wall}, at an average deviation of 1.3%. The reference that proved to be the least favorable in this profile combination was T_{avg} at an average deviation of the exact absorptivity value of 6.6%.

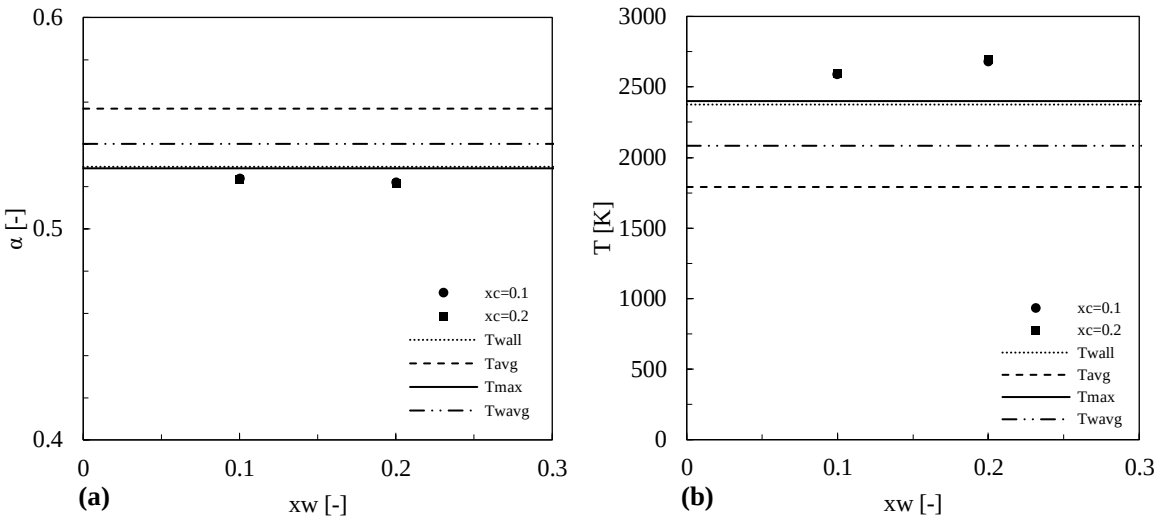

Figure 4.9 – Total absorptivity (a) and benchmark reference temperature (b) for the Profile 3 and ε-Profile 3 at different concentrations of CO_2 and H_2O.

The benchmark reference temperature for the Profile 3 and ε-Profile 3, is plotted against the selected reference temperatures on Figure 4.9(b). Again, as it occurred for the previous surface emissivity profiles, the value of T_{reb} achieved values above the maximum temperature of the domain. However, despite this, and the somewhat large deviations of the references to the T_{reb}, 9.1% for T_{max} and 10% for T_{wall}, these references proved to be great candidates to estimate the absorptivity of a surface to the conditions described in this study.

Based on the test cases, where the temperature of the domain has a maximum temperature away from the surface of interest, in this manner, close to a black emitting hemisphere border, it can be observed that the best representation of the absorptivity of the control surface is given by the temperature of the hemisphere, called in this study as T_{wall} and the maximum temperature

of the domain, T_{max}, approximated to a blackbody distribution. With these temperatures at the hemisphere border, the black hemisphere has an increased influence over the emitted radiation incident to the surface, therefore reducing the exact absorptivity value and approximating the benchmark reference temperature to the maximum and hemisphere wall. Over the entire set of cases tested in this scenario, T_{max} provided the least deviation between all of the reference temperatures studied, at an average of 1.2%, and a maximum of 2.0%. Following closely, the temperature of the hemisphere border, T_{wall}, also provided good results, at an average deviation of the LBL total absorptivity values of 1.3%, and a maximum of 2.2%. The summary of the results for the 24 test cases evaluated in this section can be seen on Table 4.

Table 4 – Summary of results for the asymmetrical temperature profiles, Profile 2 and 3.

Temp. Profile	ε-Profile	X_c [-]	X_w [-]	T_{reb} [K]	α_{LBL} [-]	δT_{avg} [-]	δT_{wall} [-]	δT_{max} [-]	$\delta T_{w,avg}$ [-]
2	ε-1	0.1	0.1	2198.3	0.546	3.5%	1.7%	1.6%	2.5%
		0.1	0.2	2232.3	0.545	3.8%	2.0%	1.3%	2.8%
		0.2	0.1	2218.8	0.545	3.7%	1.8%	1.4%	2.7%
		0.2	0.2	2254.5	0.544	4.0%	2.1%	1.1%	3.0%
	ε-2	0.1	0.1	2146.4	0.520	1.4%	0.5%	0.9%	0.9%
		0.1	0.2	2179.2	0.520	1.6%	0.7%	0.8%	1.1%
		0.2	0.1	2162.2	0.520	1.5%	0.6%	0.9%	1.0%
		0.2	0.2	2196.1	0.519	1.6%	0.8%	0.7%	1.2%
	ε-3	0.1	0.1	2146.6	0.537	2.5%	1.0%	1.6%	1.7%
		0.1	0.2	2193.5	0.536	2.8%	1.3%	1.3%	2.0%
		0.2	0.1	2156.4	0.537	2.6%	1.0%	1.6%	1.8%
		0.2	0.2	2204.5	0.535	2.9%	1.4%	1.2%	2.1%
3	ε-1	0.1	0.1	2657.2	0.530	8.2%	1.7%	1.5%	4.3%
		0.1	0.2	2722.5	0.528	8.6%	2.1%	1.9%	4.6%
		0.2	0.1	2683.1	0.529	8.3%	1.9%	1.7%	4.4%
		0.2	0.2	2751.5	0.527	8.7%	2.2%	2.0%	4.8%
	ε-2	0.1	0.1	2590.8	0.513	3.5%	0.6%	0.5%	1.8%
		0.1	0.2	2656.7	0.512	3.7%	0.8%	0.7%	1.9%
		0.2	0.1	2611.9	0.512	3.6%	0.6%	0.6%	1.8%
		0.2	0.2	2679.8	0.512	3.8%	0.8%	0.7%	2.0%
	ε-3	0.1	0.1	2589.3	0.524	6.3%	1.1%	0.9%	3.1%
		0.1	0.2	2679.0	0.522	6.7%	1.4%	1.3%	3.5%
		0.2	0.1	2602.3	0.523	6.4%	1.1%	1.0%	3.2%
		0.2	0.2	2694.5	0.521	6.8%	1.5%	1.4%	3.6%

4.3 Asymmetrical Temperature Profiles – Maximum Close To Control Surface

The final proposed scenario of this study is the evaluation of a proposed reference temperature estimation for the total absorptivity value in a domain where incident radiation has travelled a participating media composed of carbon dioxide and water vapor, which boasts a temperature profile with increasing temperature towards the control surface. In these scenarios, the temperature profile that provides this representation are the temperature Profiles 4 and 5, described by Equations 3.5 and 3.6, respectively.

Both profiles present a hemisphere temperature, T_{wall} of 400K and a maximum temperature T_{max} of 2400K. their distinction is the location where the maximum temperature is present on the domain. Profile 4 presents its value of T_{max} at the unidimensional position equal to r^*=0.3 and Profile 5 at r^*=0.1. The domain is permeated by the same constituents of the previous analyses, carbon dioxide and water vapor, at different molar concentration combinations.

4.3.1 ε-Profile 1

The evaluation of the temperature Profiles 4 starts with its coupling with the surface emissivity profile of the control surface ε-Profile 1. The resulting total absorptivity is plotted against the values obtained by the reference methodology on Figure 4.10(a). The results are disposed where the LBL obtained absorptivity values are plotted as markers for the varying values of water vapor molar concentration with a different type of marker to represent the varying molar concentration of carbon dioxide in the mixture. The reference absorptivity is plotted with lines of different styles to represent the various references used.

The exact absorptivity values obtained and presented in Figure 4.10(a) showed a reduction in the absorptivity of the surface with the increase of the optical thickness of the participating media. For the case with X_c=0.1;X_w=0.1, the exact absorptivity achieved a value of 0.711, and with X_c=0.2;X_w=0.2, this value reduced to 0.679, a reduction of 4.7%. Also from the image, it is possible to verify that these absorptivity values closely match the ones calculated by the value of $T_{w,avg}$, when assuming a blackbody distribution. This reference temperature was the one that provided the best agreement with the exact values, with a maximum deviation of 5.8% and a minimum of 1.3%.

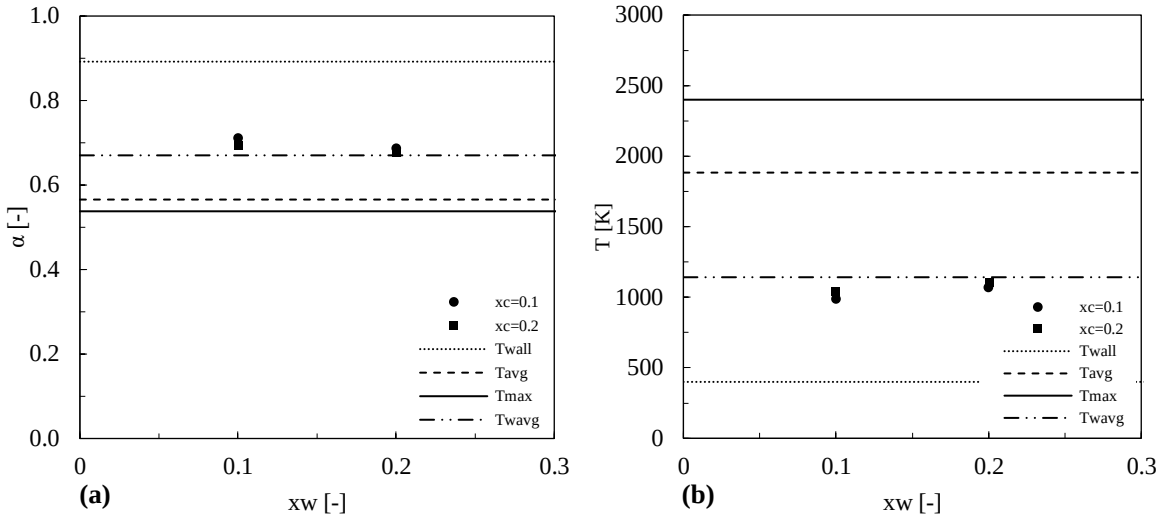

Figure 4.10 – Total absorptivity (a) and benchmark reference temperature (b) for the Profile 4 and ε-Profile 1 at different concentrations of CO_2 and H_2O.

When evaluating the reference temperatures plotted on Figure 4.10(b), the results agree with the absorptivity values, where the smallest deviation from the results of the benchmark reference temperature, T_{reb} were the ones from $T_{w,avg}$. The deviation between these temperatures achieved an average value of 8.7%, a relatively high value. However, even with this deviation, the absorptivity estimated by using this reference temperature, achieved an average deviation of only 3.3% for the four testcases plotted above.

Moving to the temperature Profile 5, with a maximum temperature closer from the control surface, at r^*=0.1, the absorptivity values obtained by solving the RTE by the LBL method are plotted as markers on Figure 4.11(a), and their respective benchmark reference temperatures are plotted also as markers on Figure 4.11(b). For the absorptivity values, again we see a reduction in its value with the increase of molar concentration of the species. The total absorptivity using the benchmark solution ranged from 0.692, for X_c=0.2;X_w=0.2 and 0.724, with X_c=0.1;X_w=0.1. From these results and comparing them to the reference absorptivity values, the ones that reached the best agreement was when using the average between the hemisphere wall temperature and the average medium temperature, $T_{w,avg}$. Using this reference the maximum deviation achieved was 5.9% for the thinnest optical media tested, X_c=0.1;X_w=0.1, and the minimum deviation achieved 1.5% for the thickest optical media, X_c=0.2;X_w=0.2.

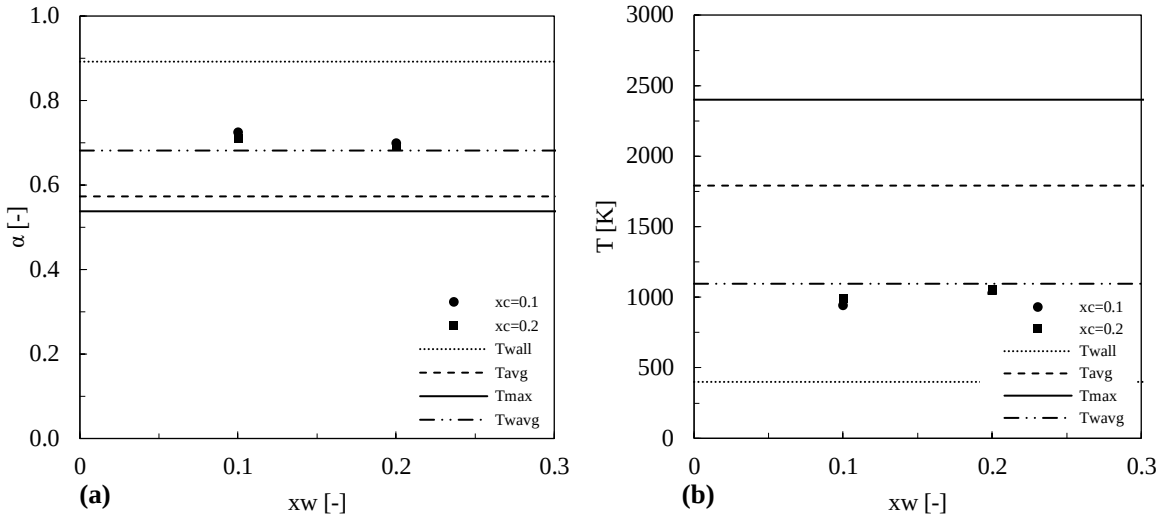

Figure 4.11 – Total absorptivity (a) and benchmark reference temperature (b) for the Profile 5 and ε-Profile 1 at different concentrations of CO_2 and H_2O.

The reference temperatures, plotted on Figure 4.11(b), corroborated with the absorptivity results, where with the increase of optical thickness of the medium where the incident radiation has travelled before hitting the control surface, the deviation between the results of T_{reb} achieved a better agreement to the reference values from $T_{w,avg}$.

4.3.2 ε-Profile 2

The temperature Profile 4 was also tested with the surface emissivity ε-Profile 2. The results for the total absorptivity of the control surface in the four testcases that this profile combination was applied can be observed on Figure 4.12(a). The results obtained showed a smaller variation in the total absorptivity range when compared to the previous ε-Profile. The total absorptivity varied from 0.575 at its lowest, and 0.584 at its highest value, for the four test cases presented. With this emissivity profile, again the reference temperature that provided the best correlation with the LBL solutions were the ones calculated via $T_{w,avg}$. The average deviation obtained using this reference was only 0.5%, therefore achieving a good correlation to the exact results.

The use of the wall temperature, as it was suggested for the previous scenario of temperature profiles, with the maximum temperature close to the black hemisphere, provided the worse deviations for the test cases. Combining Profile 4 and ε-Profile 2, the average deviation achieved a value of 38.8%, which would provide excessive errors when evaluating the heat transfer between the surface and the hemisphere border.

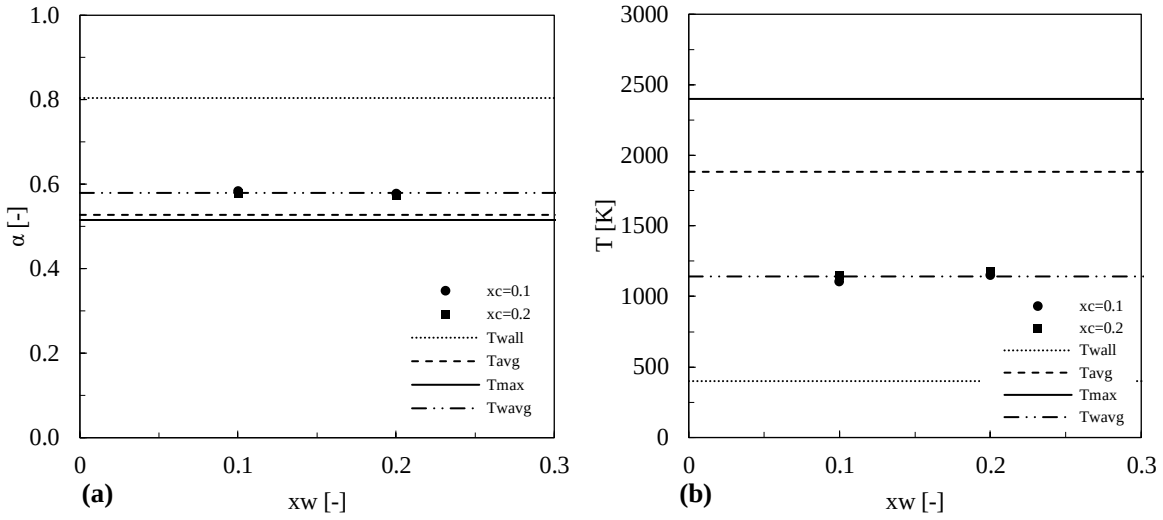

Figure 4.12 – Total absorptivity (a) and benchmark reference temperature (b) for the Profile 4 and ε-Profile 2 at different concentrations of CO_2 and H_2O.

The benchmark reference temperature, T_{reb}, plotted as markers on Figure 4.12(b), proved to be very similar to the reference $T_{w,avg}$, as was expected from the absorptivity values discussed previously. With an average deviation of 1.8%, it could represent with great accuracy the absorptivity values, estimated by the blackbody distribution. Comparing to the previous ε-Profile, number 1, the results did not show a large variation in its T_{reb} value, when the participating media was made thicker or thinner. The value of T_{reb} varied only 71.3K from its largest value, 1176.3K when the media was composed of X_c=0.2;X_w=0.2, and 1105K, for a media with X_c=0.1;X_w=0.1.

The combination of this surface emissivity profile alongside the temperature Profile 5 achieved similar results, as it is shown in Figure 4.13(a) for the total absorptivity values and in Figure 4.13(b) for the benchmark reference temperatures. There was a small variation in the total absorptivity of the test cases, ranging from 0.578 to 0.587, for the testcases where X_c=0.2;X_w=0.2 and X_c=0.1;X_w=0.1, respectively. The reference methodology that provided the best agreement to the LBL results was again $T_{w,avg}$, with an average deviation between the testcases of only 0.8%. Then it came the use of T_{avg}, at an average deviation of 8.8%, T_{max}, at 11.5% and finally the least favorable methodology to estimate the total absorptivity of the surface, T_{wall}, at 38.1%.

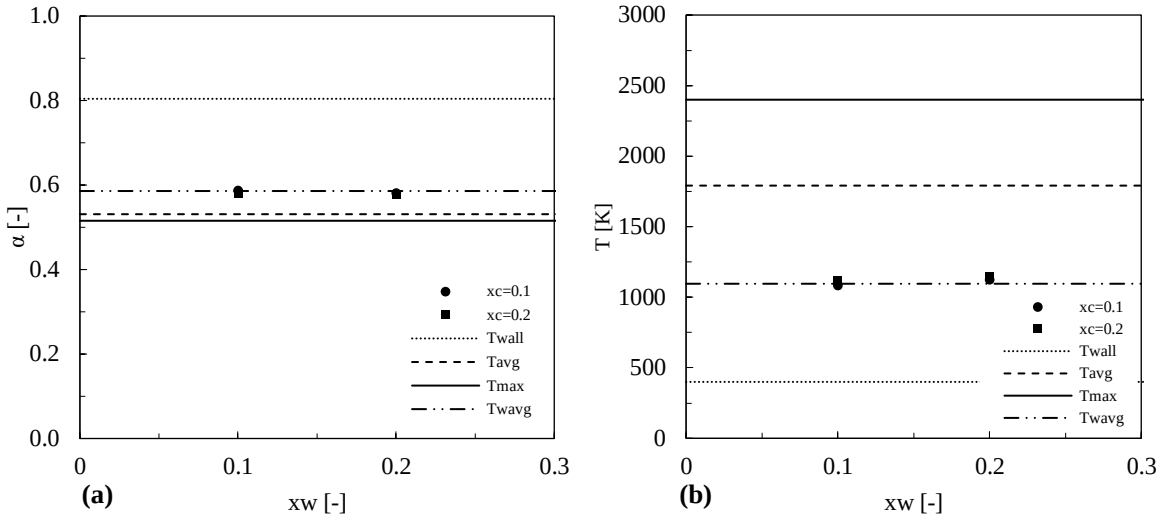

Figure 4.13 – Total absorptivity (a) and benchmark reference temperature (b) for the Profile 5 and ε-Profile 2 at different concentrations of CO_2 and H_2O.

The benchmark reference temperature for the four testcases evaluated with the combination of Profile 5 and ε-Profile 2 is plotted on Figure 4.13(b). The values obtained for T_{reb} closely matched the value for the average between hemisphere wall and average medium temperature for the Profile 5. The values for T_{reb} for the plotted testcases ranged from 1086.9K and 1152.4K, for the thinner and thicker optical media studied. Comparing these values to $T_{w,avg}$ of Profile 5, it was obtained an average deviation of 2.8%, which corresponded to the previously discussed 0.8% average deviation to the total absorptivity value. These results proved that the use of this temperature reference provides a good estimation of the absorptivity value, for this combination of profiles and mixtures of participating media.

4.3.3 ε-Profile 3

The temperature profiles 4 and 5, which provides a maximum temperature closer to the control surface, at the nondimensional distance r^*=0.3 and r^*=0.1, respectively, are now tested in combination with the surface emissivity distribution, ε-Profile 3. This profile is the representation of a fly ash coating over a given surface, with three distinct emissivity steps across the spectrum.

The first temperature profile tested is Profile 4, with the second closest maximum temperature to the control surface of all the ones tested in this study. The total absorptivity for this profile is plotted against the values calculated by the reference methodologies in Figure 4.14(a). The values for the exact total absorptivity, calculated by the LBL integration of the

RTE are plotted as markers, since they vary in respect of the participating media composition, while the reference values, dependent only on the temperature profile, are plotted as lines. Following the same organization, the values for the benchmark reference temperature, T_{reb}, is plotted against the Profile 4 reference temperatures on Figure 4.14(b).

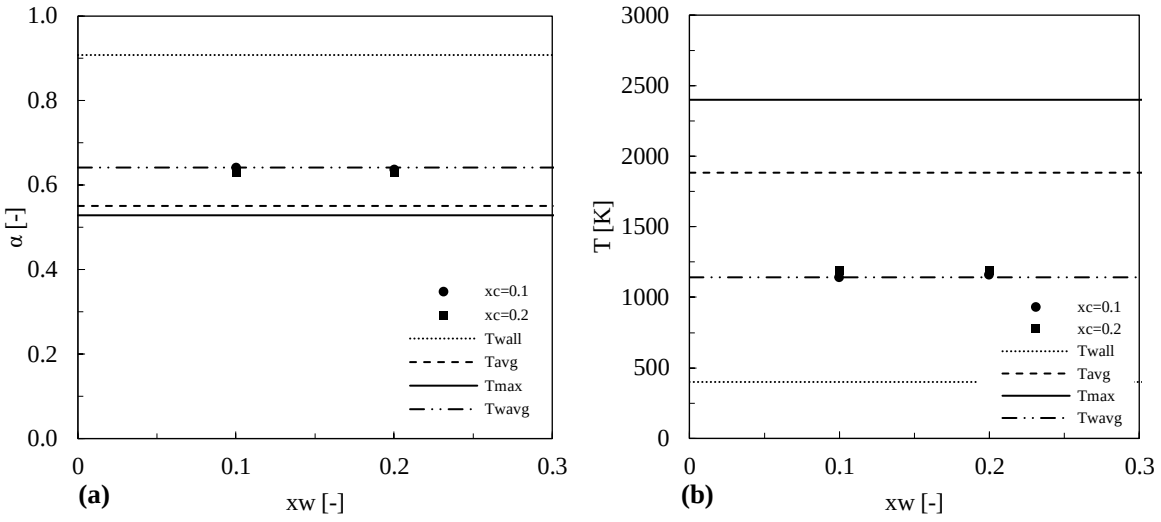

Figure 4.14 – Total absorptivity (a) and benchmark reference temperature (b) for the Profile 4 and ε-Profile 3 at different concentrations of CO_2 and H_2O.

The total absorptivity value obtained by the LBL method, as shown on Figure 4.14(a), did not achieve a large variation in respect of the molar concentration or the ratio of the mixture of participating gases. The values ranged from 0.631 for the case with X_c=0.2;X_w=0.2, to 0.642, in the case where X_c=0.1;X_w=0.1, therefore showing a slight reduction in the absorptivity of the surface with the increase of optical thickness. For this profile combination, temperature and emissivity, the reference that provided the best agreement to the exact absorptivity values was $T_{w,avg}$, This reference achieved and average deviation of 1.0% over the LBL obtained values, therefore providing a good estimate of the final absorptivity, reducing possible computational errors of the heat flux incoming and outgoing the control surface.

Looking at the benchmark reference temperature plot, on Figure 4.14(b), the values for T_{reb} ranged from 1141.4K to 1194.1K, for the thinner and thicker optical media, respectively. Corroborating to the results obtained for the total absorptivity, the reference temperature that better captured the behavior of the exact results was $T_{w,avg}$. The average deviation to the exact results, using this reference value, was 2.5%. The least effective reference for this profile combination T_{wall}, which achieved an average deviation of 65.8% to the T_{reb} and 42.9% to the resulting absorptivity value.

Moving to the evaluation of Profile 5, combined with ε-Profile 3, the results for the total absorptivity values are plotted as markers on Figure 4.15(a), while the absorptivity estimated by the reference methodologies appear as lines on the same image. The values for T_{reb} are presented in the same manner, on Figure 4.15(b).

The total absorptivity obtained with the combination of both profiles followed the same behavior, of a reduced value towards higher molar concentration of the participating species. The total absorptivity ranged from 0.635 to 0.645, for the cases where X_c=0.2;X_w=0.2 and X_c=0.1;X_w=0.1, respectively. From the image it is also possible to verify the close match to the exact absorptivity to the ones obtained by using the reference methodology with $T_{w,avg}$ as its basis. The average deviation of this method against the LBL values was 2.1%, making it an excellent reference temperature to be used to estimate the absorptivity of this surface, coupled to Profile 5.

The benchmark reference temperature of the four test cases of interest also proven to be well represented by $T_{w,avg}$, as it was expected. The average deviation of this reference temperature against the T_{reb} was 5.0%, which resulted in the aforementioned 2.1% in the total absorptivity deviation.

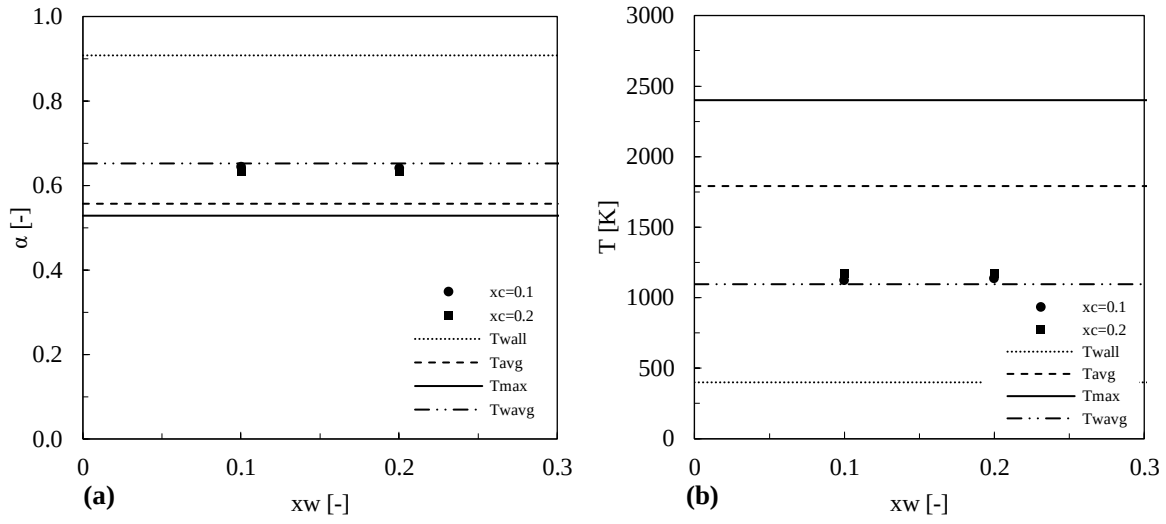

Figure 4.15 – Total absorptivity (a) and benchmark reference temperature (b) for the Profile 5 and ε-Profile 3 at different concentrations of CO_2 and H_2O.

Based on the results obtained for the temperature profiles 4 and 5, which represent the scenario where the maximum temperature of the domain is located close to the surface of interest, to have its absorptivity evaluated, the reference temperature that provided the best agreement with the exact results, obtained by the integration of the RTE over the spectrum and taking into account the spectral surface emissivity of the surface was $T_{w,avg.}$ With this reference

temperature, comparing both temperature profiles and all 3 ε-Profiles, the maximum deviation to the exact results encountered was 5.9%. The average deviation taking into account all of the test cases from all profiles was 1.85%, which is an excellent approximation of the exact results, taking into account that the reference absorptivity is estimated without the need to perform time consuming spectral integrations. The summary for all of the results obtained for this scenario can be observed on Table 5.

Table 5 – Summary of results for the asymmetrical temperature profiles, Profile 4 and 5.

Temp. Profile	ε-Profile	X_c [-]	X_w [-]	T_{reb} [K]	α_{LBL} [-]	δT_{avg} [-]	δT_{wall} [-]	δT_{max} [-]	$\delta T_{w,avg}$ [-]
4	ε-1	0.1	0.1	987.6	0.711	20.5%	25.4%	24.4%	5.8%
		0.1	0.2	1071.5	0.688	17.8%	29.7%	21.8%	2.6%
		0.2	0.1	1044.4	0.695	18.6%	28.3%	22.6%	3.6%
		0.2	0.2	1106.1	0.679	16.7%	31.4%	20.8%	1.3%
	ε-2	0.1	0.1	1105.0	0.584	9.7%	37.6%	11.8%	0.9%
		0.1	0.2	1147.8	0.579	8.8%	39.0%	10.9%	0.1%
		0.2	0.1	1147.5	0.579	8.8%	38.9%	10.9%	0.1%
		0.2	0.2	1176.3	0.575	8.3%	39.8%	10.4%	0.8%
	ε-3	0.1	0.1	1141.4	0.642	14.2%	41.5%	17.6%	0.0%
		0.1	0.2	1158.1	0.638	13.7%	42.3%	17.2%	0.6%
		0.2	0.1	1193.3	0.631	12.7%	43.9%	16.2%	1.7%
		0.2	0.2	1192.1	0.631	12.7%	43.9%	16.2%	1.7%
5	ε-1	0.1	0.1	944.2	0.724	20.9%	23.1%	25.8%	5.9%
		0.1	0.2	1030.0	0.699	18.0%	27.6%	23.1%	2.5%
		0.2	0.1	990.3	0.710	19.3%	25.6%	24.3%	4.1%
		0.2	0.2	1055.8	0.692	17.2%	28.9%	22.3%	1.5%
	ε-2	0.1	0.1	1086.9	0.587	9.6%	37.0%	12.2%	0.2%
		0.1	0.2	1126.7	0.582	8.7%	38.3%	11.4%	0.7%
		0.2	0.1	1125.2	0.582	8.7%	38.2%	11.4%	0.7%
		0.2	0.2	1152.4	0.578	8.2%	39.1%	10.8%	1.3%
	ε-3	0.1	0.1	1125.6	0.645	13.7%	40.7%	18.1%	1.1%
		0.1	0.2	1140.9	0.642	13.2%	41.5%	17.6%	1.6%
		0.2	0.1	1173.8	0.635	12.3%	43.0%	16.7%	2.8%
		0.2	0.2	1173.3	0.635	12.3%	43.0%	16.7%	2.7%

5. CONCLUSIONS

In the present work a problem regarding heat transfer by the means of thermal radiation was evaluated for a section of a hemispherical domain. This hemispherical section is bound by a black wall, representing the hemisphere edge, and a diffuse non-gray surface, called the control surface, or surface of interest. A participating medium, comprised of carbon dioxide, CO_2, and water vapor, H_2O, is permeated between both of the boundaries. The objective of the study was the evaluation of the resulting absorptivity of a given non-gray surface, subjected to incoming thermal radiation, emitted by the black hemisphere edge, travelling across a participating media with non-uniform temperature distribution across the radial axis of the domain. This evaluation was performed by integrating the radiative transfer equation (RTE) over the entire spectrum by means of line by line (LBL) integration, in order to obtain the exact absorptivity value. This value was then compared to absorptivity values calculated by assuming a blackbody distribution, Equation 3.3, using different tentative reference temperatures, taken from the temperature profile being evaluated. These tentative reference temperatures were the average domain temperature, T_{avg}, the maximum temperature, T_{max}, the hemisphere border temperature, T_{wall}, and the arithmetic average between T_{avg} and T_{wall}, called $T_{w,avg}$.

A total of three spectral emissivity profiles for the surface of interest were evaluated, all of the three were studied on previous works in the literature. In combination of these ε-Profiles, as were named in this work, four different mixtures of CO_2 and H_2O, were also evaluated. The mixtures comprised molar ratios of 1.0 and 2.0 between these species, at molar fractions of 0.1 and 0.2. And finally, five different temperature distributions across the domain were simulated, described by Equations 3.2 through 3.6, where three distinct scenarios were established. The first one comprises the symmetrical temperature distribution, where the maximum temperature lies on the midpoint between the control surface and the hemisphere border. The second and third scenarios evaluated asymmetrical temperature distributions, where the former focuses where the maximum temperature is located closer to the hemisphere border, while the latter, closer to control surface. Therefore, combining all of the variables tested in this study, a total of 60 test cases were simulated.

When evaluating the first scenario, presented in Section 4.1, for the symmetrical temperature distribution, the temperature Profile 1 was simulated, combined to the four participating media mixtures and the three ε-Profiles of interest. From obtained the results, it was found little variation on the total absorptivity of the surface for the various compositions of the participating media, with the overall behavior of a decrease of the absorptivity value with

the increase of the media thickness, that is, with the increase of the molar concentration of the species. Also, the reference that provided the best agreement to the LBL values was $T_{w,avg}$, where the maximum deviation between all the test cases for this scenario achieved a value of 4.9%, while the minimum deviation achieved 0.9%. Computing the 12 test cases in this scenario, the average deviation achieved 3.2%. Therefore, for this scenario, the use of the arithmetic average between the hemisphere temperature and the average domain temperature can be used to estimate the total absorptivity of the surface with a high degree of accuracy, improving the resulting values of heat flux calculated by the weighted-sum-of-gray-gases (WSGG) with non-gray bounding walls.

For the second scenario, where asymmetric temperature profiles with their respective maximum temperatures closer to the hemisphere edge, were evaluated it was observed an even smaller variation on the absorptivity values for the different participating media composition. For this scenario, the temperature Profiles 2 and 3 are tested, which are defined by Equations 3.3 and 3.4, respectively. These profiles have the maximum temperature occurring at the non-dimensional distance of $r^* = 0.7$ for Profile 2 and $r^* = 0.9$ for the Profile 3. The results showed that with the maximum temperature of the domain moving towards the hemisphere edge, the total absorptivity calculated by the LBL integration has the tendency to match the total absorptivity estimated by the references T_{wall} and T_{max}. For the Profile 2, both of the references provided similar accuracy to represent the real absorptivity of the surface, with an average deviation over all the test cases of 1,2% for both references. When evaluating Profile 3, the reference temperatures T_{wall} and T_{max} provided similar results, with an average deviation of 1.3% and 1.2%, respectively for the total absorptivity. Hence, using both of these references can be suggested to estimate the total absorptivity of a non-gray surface irradiated by a black one, where the incoming radiation travels across a mixture of participating media that resembles combustion products. This shows the strong influence that a black surface has over the radiative transfer in participating media.

And lastly, the evaluation of the third and final scenario, with the asymmetrical temperature profiles 4 and 5. These profiles have their respective maximum temperatures at the one-dimensional distance $r^* = 0.3$ for the Profile 4 and $r^* = 0.1$ for Profile 5, therefore having the maximum temperature closer to the control surface. From the obtained results, it was observed little variation on the total absorptivity of all three surfaces studied, with the slight tendency to increase its value with the increase of the optical thickness of the medium, similar to what happened on the first scenario. Also, from all of the results obtained comprising all three surfaces and four different mixtures, the reference temperature that provided the best

agreement to the LBL results was $T_{w,avg}$, providing an average deviation of 1.6% for the Profile 4 and 2.1% for the Profile 5, which is an excellent estimation of the exact total absorptivity of the surface and would provide little compounding errors when coupled to WSGG solutions.

5.1 SUGGESTIONS FOR FURTHER WORKS

From the proposed scenarios, it was possible to obtain a general behavior of the absorptivity for different mixtures of CO_2 and H_2O and different surface properties. However, this study could be broadened by studying more surface properties, such as selective surfaces, at different cutoff intervals. This would provide more knowledge towards the influence of the participating media at specific wavelengths.

Other possibility is the addition of soot to the participating media mixture. Soot would provide a strong influence to the results, due to its constant absorption coefficient over the wavelengths, evening the discrepancies between different concentrations of the other participating gases.

Finally, it would be of most interest to develop of a correlation, where with the input of the known variables of the problem, such as the temperature profile and either the surface properties or the constituents of the mixture, that would provide a satisfactory reference temperature. We saw on the results that the most important factor on the benchmark reference temperature result were the temperature profiles, and small variations occurred with different surface properties and gas mixtures. This would provide great results, without the need to perform the LBL testing for specific cases.

REFERENCES

BERGMAN, T; LAVINE, A. **Fundamentals of Heat and Mass Transfer**. 8th. ed. New York: Wiley, 2017. v. 148

BORDBAR, Hadi; HYPPÄNEN, Timo. Line by line based band identification for non-gray gas modeling with a banded approach. **International Journal of Heat and Mass Transfer**, v. 127, p. 870-884, 2018.

CENTENO, Felipe R. et al. Evaluation of the WSGG model against line-by-line calculation of thermal radiation in a non-gray sooting medium representing an axisymmetric laminar jet flame. **International Journal of Heat and Mass Transfer**, v. 124, p. 475-483, 2018.

CHANG, S. L.; RHEE, K. T. Blackbody radiation functions. **International communications in heat and mass transfer**, v. 11, n. 5, p. 451-455, 1984.

CENTENO, Felipe Roman et al. Evaluation of gas radiation heat transfer in a 2D axisymmetric geometry using the line-by-line integration and WSGG models. **Journal of Quantitative Spectroscopy and Radiative Transfer**, v. 156, p. 1-11, 2015.

COELHO, Pedro J. Advances in the discrete ordinates and finite volume methods for the solution of radiative heat transfer problems in participating media. **Journal of Quantitative spectroscopy and Radiative transfer**, v. 145, p. 121-146, 2014.

DA FONSECA, R. J. C. ; FRAGA, G.; FRANÇA, F. A new approach for computing the total absorptivity of non-gray surfaces in radiative heat exchanges with a participating medium. *In*: , 2019. **25th International Congress of Mechanical Engineering**., 2019.

DA FONSECA, R. J. C.; FRAGA, G. C.; FRANÇA, F. H. R. Grouping the wall spectral bands for an effective computation of the radiative transfer in participating media bounded by non-gray walls. **International Communications in Heat and Mass Transfer**, v. 120, p. 105052, 2021.

DA FONSECA, Roberta Juliana Collet et al. Application of the WSGG model to solve the radiative transfer in gaseous systems with nongray boundaries. **Journal of Heat Transfer**, v. 140, n. 5, 2018.

DA SILVA, Roger Mazurek; DA FONSECA, Roberta Juliana Collet; FRANÇA, Francis Henrique Ramos. Radiative transfer prediction in participating medium bounded with nongray walls using the SLW model. **Journal of the Brazilian Society of Mechanical Sciences and Engineering**, v. 41, n. 12, p. 1-8, 2019.

DENISON, Martin K.; WEBB, Brent W. k-distributions and Weighted-Sum-of-Gray-Gases-A hybrid model. In: **International Heat Transfer Conference Digital Library**. Begel House Inc., 1994.

DORIGON, Leonardo J. et al. WSGG correlations based on HITEMP2010 for computation of thermal radiation in non-isothermal, non-homogeneous H2O/CO2 mixtures. **International Journal of Heat and Mass Transfer**, v. 64, p. 863-873, 2013.

FERNANDES, C. S. et al. Radiative transfer calculations in fire simulations: An assessment of different gray gas models using the software FDS. **Fire Safety Journal**, v. 120, p. 103103, 2021.

FRAGA, G. C. et al. Evaluation of different gray gas formulations against line-by-line calculations in two-and three-dimensional configurations for participating media composed by CO2, H2O and soot. **Fire Safety Journal**, v. 108, p. 102843, 2019.

GORDON, I.E. *et al.* The HITRAN2020 molecular spectroscopic database. **Journal of Quantitative Spectroscopy and Radiative Transfer**, [*s. l.*], p. 107949, 2021.

Hottel, H.C.; Sarofim, A.F. **Radiative Transfer**, McGraw-Hill, New York, 1967.

HOWELL, John; MENGÜÇ, Pinar; SIEGEL, Robert. **Thermal radiation heat transfer**. New York: CRC Press, 2012.

LIU, Fengshan et al. The impact of radiative heat transfer in combustion processes and its modeling–with a focus on turbulent flames. **Fuel**, v. 281, p. 118555, 2020.

MCCLATCHEY, Robert A. et al. **AFCRL atmospheric absorption line parameters compilation**. Air Force Cambridge Research Labs HANSCOM AFB MA, 1973.

MODEST, M. F. **Radiative Heat Transfer**. [*S. l.: s. n.*], 2013.

MODEST, Michael F.; RIAZZI, Robert J. Assembly of full-spectrum k-distributions from a narrow-band database; effects of mixing gases, gases and nongray absorbing particles, and mixtures with nongray scatterers in nongray enclosures. **Journal of Quantitative Spectroscopy and Radiative Transfer**, v. 90, n. 2, p. 169-189, 2005.

MODEST, Michael F.; SINGH, Varun. Engineering correlations for full spectrum k-distributions of H2O from the HITEMP spectroscopic databank. **Journal of Quantitative Spectroscopy and Radiative Transfer**, v. 93, n. 1-3, p. 263-271, 2005.

ROTHMAN, Laurence S. et al. HITEMP, the high-temperature molecular spectroscopic database. **Journal of Quantitative Spectroscopy and Radiative Transfer**, v. 111, n. 15, p. 2139-2150, 2010.

SMITH, T. F.; SHEN, Z. F.; FRIEDMAN, J. N. Evaluation of coefficients for the weighted sum of gray gases model. 1982.

SOLOVJOV, Vladimir P.; LEMONNIER, Denis; WEBB, Brent W. Efficient cumulative wavenumber model of radiative transfer in gaseous media bounded by non-gray walls. **Journal of Quantitative Spectroscopy and Radiative Transfer**, v. 128, p. 2-9, 2013.

VERSTEEG, Henk Kaarle; MALALASEKERA, Weeratunge. **An introduction to computational fluid dynamics: the finite volume method**. Pearson education, 2007.

WANG, Liangyu; MODEST, Michael F. Treatment of wall emission in the narrow-band based multiscale full-spectrum k-distribution method. 2007.

ZHANG, Yanguo; LI, Qinghai; ZHOU, Hui. **Theory and calculation of heat transfer in furnaces**. Elsevier, 2016.

ZHOU, Yue; WANG, Qiang; HU, Haiyang. Improved spectral absorption coefficient grouping strategies in radiation heat transfer calculations for H2O–CO2-soot mixtures. **Journal of Heat Transfer**, v. 140, n. 3, 2018.